arXiv:astro-ph/0101114v1 8 Jan 2001

The Radio Galaxy Populations of Nearby Northern Abell Clusters

Neal A. Miller[1,2,3]

National Radio Astronomy Observatory[4], P.O. Box O,
Socorro, New Mexico 87801

`nmiller@aoc.nrao.edu`

and

Frazer N. Owen

National Radio Astronomy Observatory[4], P.O. Box O,
Socorro, New Mexico 87801

`fowen@aoc.nrao.edu`

ABSTRACT

We report on the use of the NRAO VLA Sky Survey (NVSS) to identify radio galaxies in eighteen nearby Abell clusters. The listings extend from the cores of the clusters out to radii of $3h_{75}^{-1}$Mpc, which corresponds to 1.5 Abell radii and approximately four orders of magnitude in galaxy density. To create a truly useful catalog, we have collected optical spectra for nearly all of the galaxies lacking public velocity measurements. Consequently, we are able to discriminate between those radio galaxies seen in projection on the cluster and those which are in actuality cluster members. The resulting catalog consists of 329 cluster radio galaxies plus 138 galaxies deemed foreground/background objects, and new velocity measurements are reported for 273 of these radio galaxies.

The motivation for the catalog is the study of galaxy evolution in the cluster environment. The radio luminosity function (RLF) is a powerful tool in the identification of active galaxies, as it is dominated by star-forming galaxies at intermediate luminosities

---

[1] Visiting Astronomer, Kitt Peak National Observatory, National Optical Astronomy Observatories, which is operated by the Association of Universities for Research in Astronomy, Inc. (AURA) under cooperative agreement with the National Science Foundation.

[2] Based in part on observations obtained with the Apache Point Observatory 3.5-meter telescope, which is owned and operated by the Astrophysical Reseach Consortium.

[3] and New Mexico State University, Department of Astronomy, Box 30001/Dept. 4500, Las Cruces, New Mexico 88003

[4] The National Radio Astronomy Observatory is a facility of the National Science Foundation operated under cooperative agreement by Associated Universities, Inc.

and active galactic nuclei (AGN) at higher luminosities. The flux limit of the NVSS allows us to identify AGN and star-forming galaxies down to star formation rates (SFR) less than $1 M_{\odot}$ yr^{-1}. This sensitivity, coupled with the all-sky nature of the NVSS, allows us to produce a catalog of considerable depth and breadth. In addition to these data, we report detected infrared fluxes and upper limits obtained from IRAS data. It is hoped that this database will prove useful in a number of potential studies of the effect of environment on galaxy evolution.

Subject headings: catalogs — galaxies: distances and redshifts — galaxies: clusters: general — galaxies: radio continuum

1. Introduction

One of the major areas of research in extragalactic astronomy today is that of the effect of environment on the evolution of galaxies. The uniqueness of the cluster environment has been a major driver in such studies. Within a reasonable field size, clusters provide enough galaxies to draw statistically-significant conclusions over a broad range in local galaxy density. In addition, the diffuse intracluster medium (ICM) of clusters provides another influence on the evolution of member galaxies, as seen in the HI deficiency of cluster spirals and their often disturbed HI morphologies (Haynes et al. 1984).

Naturally, evolutionary studies have also examined the differences between clusters at moderate redshift with those seen nearby. Butcher & Oemler (1978) noted that the fraction of blue galaxies in clusters increases as one moves to higher redshifts. Presumably, this increase in blue fraction is the result of more active episodes of star formation in galaxy clusters at earlier epochs. While blue colors provide only a rough diagnostic of star formation, more accepted star formation indicators have been applied to clusters at low redshift. Kennicutt et al. (1984) investigated the Hα properties of several nearby clusters (Cancer, Coma, A1367, and the Virgo cluster Hα data from Kennicutt & Kent 1983). They tentatively concluded that the star formation rates (SFR) derived from Hα were slightly lower in clusters than field galaxies. The uncertainty in this conclusion was due to the strong dependence of Hα emission on Hubble type and the difficulty in assigning such classifications to the cluster galaxies. Furthermore, they identified several galaxies whose interesting properties were rarely seen outside of the cluster environment. These were generally faint, irregular galaxies with very strong Hα emission and radio emission. They also noted that spiral galaxies in the core of Virgo seemed to have lower star formation rates.

Radio emission also happens to be an excellent probe of star formation. It is believed that as massive stars die in supernovae, they eject cosmic ray electrons which then spiral in the host galaxy's magnetic fields and emit synchrotron radiation (see review in Condon 1992). The lifetimes of such relativistic electrons are of the order 10^8 years, and since they result from massive stars with short lifetimes themselves the radio emission is an indicator of nearly present star formation.[5] Furthermore, the radio power seems to be directly related to the SFR. The radio luminosity function (RLF) at 1.4GHz represents a smooth continuum running from normal quiescent galaxies, to galaxies undergoing increasing levels of star formation, to relatively radio-weak AGN (e.g., Seyferts), and on to the rare yet extremely radio-powerful AGN (the classic Fanaroff-Riley I and II sources; Fanaroff & Riley 1974). The overall shape of the RLF closely resembles that of the more familiar optical luminosity function, and in each case the Milky Way lies very close to the knee in the LF.

In addition to the influence on star formation, numerous studies have investigated the effect of the cluster environment on active galactic nuclei (AGN), notably the powerful radio galaxies. The radio emission from these galaxies often extends well beyond their optical boundaries, out to hundreds of kiloparsecs. One might expect the ICM in clusters to confine the radio plasma from these galaxies, thereby affecting the total power of cluster radio galaxies. However, the RLF has not been shown to differ in clusters vs. the field (Fanti 1984; Ledlow & Owen 1996), nor does the probability for a galaxy to emit radio depend on cluster galaxy density (Zhao et al. 1989; Ledlow & Owen 1995a).

Consequently, a comprehensive catalog of nearby cluster radio galaxies is a useful tool in the study of the effect of the cluster environment on galaxy evolution. A large, comprehensive database will allow for more statistically robust studies of the above questions, plus detailed investigations of galaxy evolution in a range of cluster environments.

In order to detect the more normal star-forming galaxies as well as the more radio-powerful AGN, sensitive radio maps are required. In the past, such sensitivity could be achieved reasonably easily for nearby clusters but the beam size of the radio observations restricted such studies to only the cores of such clusters. Technological advances have solved these problems. Lower noise radio receivers have reduced the time requirements for all-sky surveys at good sensitivity, and computing power has followed suit and made reduction of such a large volume of data feasible. Furthermore, procedures for creating near-uniform sensitivity mosaics of the radio data which accurately account for the problems inherent to wide-field radio imaging have been developed. One result of these advances is the NRAO VLA Sky Survey (NVSS: Condon et al. 1998), which covers the entire sky north of $\delta = -40$ at a frequency of 1.4 GHz. Performed with the VLA in D-array, it has a resolution of about $45''$ and is sensitive enough to detect sources down to $S \approx 2.5$ mJy.

Within this paper, we use the NVSS to identify the radio galaxies in a sample of nearby clusters. The all-sky nature of the NVSS allows us to catalog radio galaxies out to great distances from the more well-studied cores of clusters. Adopting $H_o = 75$ km s^{-1} Mpc^{-1} and $q_o = 0.1$, we identify NVSS radio galaxies out to 3 Mpc from the cores of nearby clusters. This corresponds to approximately four orders of magnitude in galaxy density, thereby probing regions from the densest centers of clusters to those consistent with the average density of the field. The excellent sensitivity of the NVSS ensures that the identified galaxies include normal star-forming galaxies as well as powerful AGN. For example, at $z = 0.015$ (about the nearest cluster in our sample) the flux limit of the NVSS corresponds to about 1×10^{21} W Hz^{-1}, which means we detect objects with SFR$\gtrsim$ 0.5M$_\odot$ yr^{-1} (see Carilli et al. 2001, for the equation relating radio luminosity to SFR). Even at our redshift cutoff the NVSS detects galaxies with SFR$\gtrsim$ 3M$_\odot$ yr^{-1}. The beam size of the NVSS is comparable to that of a spiral galaxy disk for the redshifts investigated, insuring that even diffuse radio emission spread over the disks of normal star-forming galaxies is detected.

---

[5] Note that optical indicators of SFR, in particular Hα, have timescales around 10^7 years. However, the remarkable correlation of radio emission and Hα emission seen for star-forming galaxies suggests that the overall duration of episodes of star formation makes this distinction minor.

In addition to the radio fluxes, we report both new and old data that are useful in investigating the effect of the cluster environment. We have compiled far infrared (FIR) data for all the radio galaxies, utilizing the IRAS Faint Source and Point Source Catalogs (FSC and PSC, respectively). In the event such data are not available, we have used IPAC's *xscanpi* software to estimate fluxes from cross scans of the IRAS satellite. Perhaps most importantly, we report velocities for all but two of the identified radio galaxies, with many of these velocities arising from new observations. These data differentiate the true cluster radio objects from those merely seen in projection on the cluster.

The paper is organized as follows. In section two, we present the cluster sample and summarize the procedure we have used to identify the candidate radio galaxies in each cluster. The compilation of public data, including velocities and FIR fluxes, is also discussed in this section. In section three, we discuss the spectral observations we have made for many of the candidate radio galaxies. This includes a summary of where, when, and how the data were collected, and our reduction and analysis procedures. Section four presents the results, in the form of complete tables for both the confirmed cluster radio galaxies and those radio galaxies deemed foreground or background objects. In section five we conclude with some simple conclusions and an overview of potential uses for the data.

2. Sample Identification

2.1. Cluster Sample

The galaxy clusters analyzed are taken from the catalog of Abell et al. (1989) (ACO). This revision of Abell's original catalog (Abell 1958) contains 4073 potential clusters of galaxies, as determined from inspection of the Palomar Observatory Sky Survey (POSS I) plates and the Southern Sky Survey. We have imposed a systemic recessional velocity cutoff of 10,000 km s^{-1} ($z = 0.033$), as beyond this redshift the sensitivity of the NVSS would no longer allow us to detect galaxies with massive SFRs below about 2 M$_\odot$ yr^{-1}. In addition, we have accepted only clusters with positive declinations although the NVSS coverage extends down to $\delta \sim -40$. While there are a large number of clusters meeting these criteria, many possess fairly faint magnitudes for their tenth-brightest member despite supposedly low systemic redshifts, making them somewhat uncertain. Furthermore, the areal coverage required to survey radial extents of 3 Mpc becomes prohibitively large at low redshift. As a result, we have settled on the 18 ACO clusters presented in Table 1.

The sample spans a range of cluster environments. Half of the members are poor clusters of richness class 0 (see Abell 1958), while the other half are fairly rich systems. In fact, four of the clusters are of richness class 2, which means that they are richer than approximately 95% of all clusters. There are examples of cooling flow clusters (A426 and A2199), clusters with features suggesting recent large-scale interactions such as cluster-group mergers (A400, A1656, and A2634), and a number of clusters which together make up superclusters.

2.2. Generating Optical Galaxy Lists

The optical identifications are based on the Second Palomar Observatory Sky Survey (POSS II: Reid et al. 1991). The overwhelming success of the POSS I coupled with advances in photographic emulsion led to the initiation of this study, which offers both improved resolution and deeper limiting magnitudes than the original survey ($1'' \; pixel^{-1}$ vs. $1.7'' \; pixel^{-1}$, and $R_c(lim) \sim 21$ vs. $R_c(lim) \sim 20$, respectively). We have used the IIIa-F images ($\lambda_{eff} \sim 6500$Å, bandwidth ~ 1000Å) in their digitized form[6] for our optical identifications, positions, and approximate R-band magnitudes.

For each cluster, we adopt a center position and system redshift (see Table 1). Then, a grid of overlapping square maps sufficient to cover the entire cluster out to 3 Mpc in radial distance from the assigned center are obtained. Each image then has a coordinate system applied using the plate solutions found in the headers of the FITS images, and the resulting coordinates are generally accurate to about $1''$ (Deutsch 1999). SAD ("Search And Destroy"), a task within NRAO's Astronomical Image Processing System (AIPS), is then used to identify all objects significantly above the noise level on POSS II images. As stars may be represented by (often saturated) point source profiles and galaxies are fainter, more extended objects, we make a strong first cut at galaxy/star segregation using the source fluxes and widths reported by SAD. SAD also reports the centers of the identified objects, as determined by the best-fitting Gaussian to the real data.

We then calculate the equivalent R-band magnitudes for the identified galaxies. All our magnitudes are calculated for the Gunn-Oke aperture (Gunn & Oke 1975), which corresponds to a linear aperture radius of 13.1 kpc (for $H_o = 75$ km s^{-1} Mpc^{-1}) at the systemic redshift of the cluster. To establish the magnitude zero point, we have bootstrapped the POSS II images to the photometry reported in Ledlow & Owen (1995b). This study reported photometric results for the powerful radio galaxies in ACO clusters, and as a result there is usually a galaxy or two in each of our clusters that has a published magnitude from which to work. In the event that there is no galaxy in common between the Ledlow & Owen photometry and our clusters, we have adopted a magnitude zero point of 30.10, about the global average for the common galaxies in the entire sample. The adopted magnitude zero point for each cluster may also be found in Table 1. Once these parameters are established, the aperture photometry is preformed automatically using the PHOT task in IRAF. The local background for each galaxy is calculated using a large annulus centered on the galaxy. The subsequent magnitudes are generally accurate to within 0.5 magnitudes, with this error representing roughly equal contributions from uncertainty in the magnitude zero point and photometric measurement.

---

[6] The Digitized Sky Surveys were produced at the Space Telescope Science Institute under U.S. Government grant NAG W-2166. The images of these surveys are based on photographic data obtained with the Oschin Schmidt Telescope on Palomar Mountain and the UK Schmidt Telescope. The plates were processed into the present compressed digital form with the permission of these institutions.

To remove probable background objects and reduce the galaxy list to those most likely to be associated with each cluster, we discard the fainter objects. Our cutoff magnitude is $m^* + 2$, where we have assumed that $M_R^* = -22$ (Owen & Laing 1989) and the attendant m^* is calculated based on the systemic velocity of each cluster. In addition, we allow for Galactic extinction in the direction of the cluster (see Table 1).

2.3. Identification of Radio Galaxies

For any given radio source, there is a definable probability that it will randomly be associated with an optical galaxy. This probability is a function of radial separation, such that perfect positional coincidence has a very high probability of representing true association whereas larger separations are more likely to be the result of common chance. The probability that a radio source is randomly associated with an optical counterpart within separation r is

$$P(< r) \;=\; 1 \;-\; \exp(-\rho\pi r^2) \tag{1}$$

where ρ is the density of background objects (i.e., the average density of optical galaxies about the radio objects).

In creating our list of radio galaxies, we have imposed a probability of 0.5%, or statistically, we expect that fewer than 1 out of every 200 identified radio galaxies is the result of chance superposition. To determine ρ we take the NVSS catalog list of radio sources in the area surveyed for each cluster and calculate the average density of objects from our optical galaxy list about each radio source. Given these parameters we solve Equation 1 for the search radius to use in each cluster. As this is done for each cluster, the search radius from cluster to cluster is a variable but is generally in the range of $15''$ to $35''$. Then, if the nearest optical galaxy for a given radio source is within this radius we associate the pair as a radio galaxy.

While many studies simply use a fixed radio and optical separation to identify radio galaxies, we feel the probabilistic approach is better suited to this study. First, since the clusters are at different redshifts a fixed angular separation results in a more restrictive acceptance criterion for nearby galaxies. Optically, the nearer galaxies in the sample can easily span two arcminutes, whereas the farthest galaxies are well under an arcminute in extent. Relative errors in the galaxy center positions are therefore more likely to be larger for nearby galaxies, so a larger search radius is desirable. More importantly, our procedure consistently handles variations from field to field. For example, any errors in astrometric registration are accounted for in finding the search radius for that specific field.

After these automated routines are completed, the entire field for each cluster is inspected by eye. NVSS images are obtained, and overlays of NVSS contours on the POSS II images are created and inspected. This step is time consuming but serves a number of important functions. First, the galaxy/star identification algorithm is not perfect and a number of apparent close binary stars are labelled galaxies. These objects may be easily identifed and removed from the optical galaxy list during visual inspection. Second, any galaxy that was missed for some reason by the automated procedures may be added in by hand. This type of error rarely occurred except in the cases of very large galaxies. Once these corrections have been made, the updated optical list and the NVSS Catalog list are again correlated with one another to determine the semi-final list of radio galaxies for each cluster. In this step, the search radius is recalculated to reflect the updates in the list of optical galaxies.

The final purpose of the visual inspection is the identification of powerful, extended radio sources. Since the NVSS Catalog was generated by an automated procedure which fit peaks in radio emission, extended sources are frequently fit by multiple sources with smaller fluxes. There are two net effects of this on our radio galaxy identification procedure. First, the fluxes for some of our radio galaxies will be under-represented by their fluxes in the NVSS Catalog should the radio source be resolved into multiple components. For these, we have used the actual NVSS images to measure the net flux associated with the radio galaxy. Second, for some sources the fitted peak in the NVSS Catalog lies outside our adopted search radius (for example, see 3C465 in A2634). As these powerful radio galaxies are an important portion of our radio galaxy catalog, it is vital that they be identified. Table 2 lists all of the identified candidates for such inclusions along with the separations between our optical positions and the nearest NVSS Catalog radio position, their net fluxes as measured off the NVSS images, and their common name where applicable. Overlays of the NVSS contours on the POSS II images for candidate extended radio sources are presented in Figure 1.

As the resolution of the NVSS is about $45''$, we have used Faint Images of the Radio Sky at Twenty Centimeters (FIRST, Becker et al. 1995) to investigate the extended sources whenever such images were available. FIRST is also being undertaken with the VLA, using the same pointing grid and mosaic strategy as the NVSS but in the longer baseline B-array. As such, it provides a resolution of about $5''$ with 5σ detections near 1 mJy. The smaller beam size makes it less sensitive to diffuse, extended sources yet it is useful in demonstrating that some of our apparent extended

NVSS radio galaxies are chance projections of more compact objects at higher redshift. Figure 1 presents the FIRST images for the candidate extended sources, and Table 2 indicates whether such sources were accepted in the final list of radio galaxies.

This procedure was applied to all the clusters, with one minor exception. The NVSS radio image of A426, the Perseus cluster, is dominated by the extremely powerful radio galaxy NGC1275, which is also known as Perseus A or 3C84. Since the core of this source is unresolved and at a radio power of nearly 25 Jy, there are significant artifacts in the central region of this cluster. Therefore, we have used the radio galaxy identifications of Sijbring (1993) within $0.5h_{75}^{-1}$Mpc of Perseus A. The radio galaxies chosen in this way were required to be consistent with the rest of this study, in that we accepted only the Sijbring radio galaxies with fluxes which should render them detected by the NVSS.

3. Characterization of Radio Galaxies

3.1. Infrared Data

A useful characterization of galaxies with radio emission is provided by their far infrared (FIR) emission. For normal star-forming galaxies as well as those actively involved in starbursts, the radio and FIR fluxes are strongly correlated (see review in Condon 1992). While the two types of emission are different (non-thermal for the radio and thermal for the FIR), the root cause in each case is massive stars. In the radio, as these massive stars die in supernovae they accelerate electrons which spiral in the galaxy's magnetic fields and emit synchrotron radiation. During their brief lifetimes, the massive stars are the primary heaters of dust in HII regions. As a result, galaxies which are presently forming massive stars follow the FIR-radio correlation.

A useful measure of the FIR-radio correlation is the statistic q, defined by Helou et al. (1985) as

$$q \equiv \log\left(\frac{FIR}{3.75\times10^{12} W\ m^{-2}}\right) - \log\left(\frac{S_{1.4GHz}}{W\ m^{-2}\ Hz^{-1}}\right) \qquad (2)$$

where FIR is defined as

$$\left(\frac{FIR}{W\ m^{-2}}\right) \equiv 1.26\times10^{-14}\left(\frac{2.58 S_{60\mu m} + S_{100\mu m}}{Jy}\right). \qquad (3)$$

The numerical terms in the FIR expression are used to convert the IRAS flux densities into a representation of total flux between about 40μm and 120μm. Thus, q is a logarithmic measure of the FIR/radio flux density ratio. For a wide variety of star-forming galaxies (including E's and S0's with active star formation), the distribution of q is very narrow. The median value is about

2.3, with a standard deviation of around 0.2. Consequently, q may be used to characterize radio galaxies as either star-forming or AGN. In AGN, there is effectively an excess of radio emission relative to FIR emission leading to low values of q.

We have used the NASA/IPAC Extragalactic Database (NED)[7] to collect IRAS data on all galaxies in the sample. NED contains the information from the IRAS Point Source and Faint Source Catalogs (PSC and FSC, respectively), so galaxies with such FIR fluxes will be so marked. However, lack of a NED IRAS entry does not necessarily imply that the galaxy in question was not detected by IRAS. Some galaxies with detected IR emission were left out of the catalogs on account of their proximity to other IR sources.

For all galaxies lacking NED FIR entries, we have used IPAC's *xscanpi* software to estimate the 60μm and 100μm fluxes. *xscanpi* performs coaddition of all IRAS scans across a given position and returns information such as peak flux, integrated flux, and rms noise. It is thereby useful in determining fluxes for confused or faint sources, and for determining upper limits to FIR fluxes. The data are presented for four different averaging schemes, corresponding to weighted mean, straight mean, median, and noise-weighted mean. We have adopted the median results as they are purported to be "the most consistently 'good' estimator... chiefly because of the non-Gaussian nature of noise in the IRAS data."[8] The flux estimates we adopt correspond to a spatial bandpass equivalent to that of the IRAS resolution at each 60μm and 100μm.

In addition to the radio galaxies lacking NED FIR entries, around 10% of the radio galaxies are IRAS Point Source Catalog (PSC) objects with 60μm detections and 100μm upper limits (90% confidence). We have also used *xscanpi* to re-evaluate the 60μm and 100μm flux densities of these galaxies, as the cross scan addition reduces the noise and can provide firmer 100μm flux densities. Figure 2 depicts the q values determined from the PSC catalog compared with their corresponding cross scan addition results. As expected, the q values show a near one-to-one correspondance but with the PSC-derived upper limit values producing slightly higher q. In general, the addscan fluxes for sources detected at both 60μm and 100μm are consistent with the PSC fluxes to within a few percent (Saunders et al. 2000). The addscan fluxes are on average slightly higher because the scan addition counts interacting systems as single sources whereas they may be separated into distinct components in the PSC.

Using these values for the 60μm and 100μm fluxes in conjunction with the NVSS radio data, we calculated q values for all of the identified radio galaxies. It should be noted that these q values frequently represent upper limits on account of uncertainty in the IR fluxes. Nevertheless, they may be used in conjunction with the absolute radio powers of the sources to obtain a good idea of the nature of the radio source, star-forming galaxy or AGN. Figure 3 demonstrates this in the form of a histogram of q values for the confirmed cluster members (see next section). It can easily be seen that the distribution of q values peaks at 2.3, and consequently that the radio emission for the majority of the identified galaxies originates from star formation. This statement is valid in the statistical sense, in that the FIR and radio emission of AGN are also correlated but exhibit a greater scatter in their q values. Thus, while most AGN have $q \lesssim 2$ their distribution includes some galaxies with q values representative of normal star-forming galaxies. Conversely, some star-forming galaxies in clusters are radio overluminous (i.e., lower q). These topics are addressed in Miller & Owen (2001).

---

[7] The NASA/IPAC Extragalactic Database (NED) is operated by the Jet Propulsion Laboratory, California Institute of Technology, under contract with the National Aeronautics and Space Administration.

[8] http://www.ipac.caltech.edu/ipac/iras/scanpi_interp.html

3.2. Velocity Data

In order to confirm or refute the cluster membership of the identified radio galaxies, velocity measurements are necessary. We have relied upon the published velocity dispersions of Struble & Rood (1999) to assess cluster membership. These velocity dispersions were calculated using all publicly-available redshift measurements as of December 1998, and are listed along with the other adopted cluster parameters in Table 1. Galaxies whose velocities differ from the adopted cluster systemic velocity by less than three times the adopted velocity dispersion were considered to be cluster members. Those failing this criterion were designated non-cluster members, and are assumed to be either foreground or background objects.

In searching NED for IR data on the galaxies, we have also noted the redshifts whenever such data were available. However, due to the large angular extent of our study velocity data were not available for many radio galaxies. In addition, many of the radio galaxies were deemed interesting for specific science questions that required optical spectra. Consequently, we have obtained long-slit optical spectra for many of the galaxies within the sample.

3.2.1. Optical Spectroscopy Observations

The spectra were obtained during the course of several observing runs at Apache Point Observatory (APO) and Kitt Peak National Observatory (KPNO). The APO observations were made using the ARC 3.5-meter telescope with the Double Imaging Spectrograph (DIS), while the KPNO observations were made using the 2.1-meter telescope with the GoldCamera Spectrograph (GCAM). In addition to the objective of determining accurate radial velocities, we also desired high signal-to-noise spectra for line ratio diagnostics and other analyses. Consequently, we employed moderate resolution gratings which provided wavelength coverage of the entire optical window and at a resolution sufficient to resolve line complexes such as Hα and [NII]. Dates and relevant parameters of the observations are provided in Table 3.

Thanks to the large range in right ascension of the sample, we were always able to observe the target radio galaxies at low airmass. As a result of this and to increase our efficiency in collecting the spectra, we performed no slit rotations. In each observation, we simply aligned the slit with the nucleus of the target galaxy. Once the target was so acquired, the duration of the exposure was usually fifteen minutes. In some instances, we reduced the exposure time for particularly bright galaxies or lengthened the exposure times when there was suspected cirrus.

3.2.2. Spectroscopic Data Reduction and Velocity Measurement

The data were reduced in the usual manner using IRAF. The two-dimensional spectra were overscan subtracted, bias subtracted, and flat fielded using stacked frames of calibration quartz lamps, with twilight frames being used to correct for the illumination pattern of the slit. The wavelength scales were derived using observations of HeNeAr lamps. To account for telescope flexure and temperature changes throughout the nights, at least one set of calibration lamps was taken at each cluster. The long slits provided plenty of area to perform accurate sky subtraction.

Velocity measurement followed one of two paths. Since many of the galaxies are star forming, they possessed a number of emission lines. Whenever present, we measured the velocities using these lines. Line locations were determined using Gaussian fits, with each detected emission line receiving equal weight in the determination of the galaxy's recessional velocity and associated uncertainty. The detected lines are listed along with the resultant redshifts in Table 4. Repeated observations of velocity standard stars on each evening of the run showed agreement within about 20 km s^{-1}.

For many of the galaxies, emission lines were not present or were too noisy to be definitive in velocity measurement. Additionally, we required more than one emission line (or complex, such as Hα–[NII]) to report an emission line velocity. In these cases, we have used the IRAF task FXCOR. This task utilizes a fourier cross correlation procedure (Tonry & Davis 1979) to match a template absorption line spectrum with known heliocentric velocity to the target spectrum. We used the radial velocity standard stars HD132737 and HD090861, obtained during the first and second KPNO observing runs respectively, as our template spectra. We required a fit which produced R greater than five (see Tonry & Davis 1979), though in nearly all cases the correlation was much better than this and typically R was around twenty. The resulting heliocentric redshifts and associated errors are presented in Table 4. Measurements determined via this cross correlation technique are those for which either no emission lines or emission lines in parentheses are listed in Table 4.

4. Results

The total number of radio galaxies identified by the procedures outlined above was 467. Of these, 329 were deemed cluster members by their measured velocities, including three galaxies for which no accurate velocity measurement was obtained. These radio galaxies are listed by cluster in ascending order of right ascension in Table 5. In addition to the optical positions of the radio galaxies, a number of valuable parameters are provided. These include the redshift, R-band magnitude, radio and infrared flux densities (from the NVSS and IRAS, respectively), and q value. Table 6 presents the same information for the non-cluster radio galaxies.

A few things should be noted about the values presented in Tables 5 & 6. The coordinates for the radio galaxies (columns 2 and 3) correspond to the optical centers of the host galaxies, as measured from the POSS II images. These measured positions correspond to the peak of the best-fit Guassian to the galaxies, and as noted the astrometric solutions for the images are generally only good to within about $1.5''$(Deutsch 1999). For those galaxies for which we have not obtained an optical spectrum, the listed redshifts were obtained from NED. The reader is directed to this resource for specific references for these values as well as their attendant errors. As noted in Section 2, the apparent magnitudes presented in column 5 should be accurate to within 0.5 magnitudes. As they are calculated using the Gunn-Oke aperture, they fall short of the full galaxy magnitude for the larger galaxies. Some of the FIR fluxes reported in columns 7 and 8 should be taken with caution. Our reliance on the median averaging in *xscanpi* combined with the flux estimator assuming a fixed signal range means we sometimes get detected fluxes for sources which are in actuality only nearby a true source. These sources can usually be identified as those within a few arcminutes of one another, and their q values should be viewed in this light. Lastly, there are no IRAS scans in the direction of A1267 and hence there are no reported FIR flux densities or q values for this cluster.

Simple conclusions may be drawn from Table 5. As would be expected, the four clusters possessing the most radio galaxies are the richness class 2 clusters. A426 (Perseus) has 43 confirmed radio galaxies, making it the richest system in the sample. However, the proximity of A426 coupled with the flux-limited radio data contribute strongly to this result. Applying a uniform radio luminosity cut-off makes A1656 (Coma) as rich as A426 in radio galaxies. Several of the richness class 0 clusters have very few radio galaxies and likely represent chance superpositions of unrelated systems. For example, 10 out of 17 identified radio galaxies in the field of A1267 turned out to be background objects. The distributions of the radio galaxies in individual clusters also appear to reflect larger scale structures, often aligning with nearby clusters or including distinct sub-clumps within the clusters.

A number of interesting things about the non-cluster radio galaxies can be seen from Table 6. These galaxies are frequently clumped in velocity space, indicating the presence of background clusters which may or may not be associated with Abell clusters. In some instances, it seems likely that cluster identified by Abell strictly on the basis of magnitudes represents the superposition of potentially unrelated systems. For example, A2162 contains only four radio galaxies consistent with the cluster at $z \sim 0.03$, whereas an additional six radio galaxies are at $z \sim 0.05$ (sometimes referred to as A2162N). In other cases, our identification procedure has resulted in the inclusion of background Abell clusters - such as A1213, concentrated in two clumps located in the northeast and southeast of A1185. While such systems may trace larger-scale structures, it appears that the majority of the galaxies labelled non-cluster are background radio galaxies. Only 18 of the 138 non-cluster radio galaxies lie between three and five times the velocity dispersion of their projected cluster, with most of the remaining 120 at much greater velocities.

As might be expected, many of these background radio sources are also detected in surveys at other frequencies such as the 87GB Catalog (Gregory & Condon 1991). As the galaxies apparently associated with these radio sources formally met our selection criteria, we obtained optical spectra for them and confirmed that they are, in fact, powerful radio galaxies at higher redshift. Included among these are several galaxies which lay just outside our $3h_{75}^{-1}$Mpc search radius and are consequently left out of Table 6, but may be found in the spectroscopy results of Table 3. For example, the source 113049+252436 was found to be at a redshift of 0.1444 and consequently have a radio power of $10^{24.5}$ W Hz^{-1}.

We also note a few cases where powerful known radio galaxies lie just outside the $3h_{75}^{-1}$Mpc limit of our sample but at redshifts consistent with cluster membership. 3C76.1 is at a projected separation of $\sim 3.3h_{75}^{-1}$Mpc from the center of A397 and at the same redshift as the cluster. B2 1108+27 also seems to be associated with A1185, lying $\sim 3.5h_{75}^{-1}$Mpc from that cluster's core and at essentially the same redshift. Lastly, we find that UGC02755 appears to be associated with a powerful radio source. This galaxy is barely excluded from our sample, as it is $3.01h_{75}^{-1}$Mpc from the center of A426. The presence of powerful radio galaxies such as these at significant distances from the centers of these Abell clusters is strongly suggestive of the importance of large-scale structure in the formation and evolution of radio galaxies.

In addition to the summary information presented in Table 5, we have computed absolute quantities for the cluster radio galaxies. In these calculations we have assumed that all of the galaxies within a cluster lie at the same distance, which was determined from the cluster systemic velocity adopted in Table 1. Hence, we assume that the galaxies are bound cluster members and that the redshift range within each cluster is simply the result of peculiar velocities. Table 7 presents the absolute R-band magnitude, 1.4 GHz radio power, and FIR luminosity (derived based on Equation 3) for each cluster radio galaxy.

The utility of the absolute quantities is perhaps greatest for investigation of the SFRs of the cluster galaxies. Typically, the 1.4 GHz radio luminosity is converted to a SFR using the relationship found in Condon (1992). This relationship is derived empirically using the radio luminosity and supernova rate of the Milky Way, and uncertainty in such quantities translates to uncertainty in derived SFRs. In comparison to other wavelength estimators of SFR, the radio determination likely produces higher SFRs (e.g., Haarsma et al. 2000, find the radio SFR to be several times greater than extinction-corrected optical SFRs). An alternate derivation of the relationship between radio luminosity and SFR which yields values more in line with optical results is presented in Carilli et al. (2001). In the current paper, we have adopted this relationship. Using the flux limit of the NVSS for the range in redshift covered in this catalog, galaxies with SFR$\gtrsim 0.5 - 2.7$M$_\odot$ yr^{-1} are detected.

5. Conclusions

We have presented a comprehensive catalog of the radio galaxies in nearby Northern Abell clusters. This catalog is complete down to relatively low radio powers, and our collection and compilation of velocity data ensures that the true cluster members are separated from those radio galaxies viewed in projection. In conjunction with these data, we report FIR fluxes and corresponding values of q, a parametrization of the FIR-radio correlation. Using the cluster velocities, we have compiled a list of the absolute magnitudes, radio powers, and FIR luminosities of the confirmed cluster radio galaxies.

This paper is the result of many nights of spectroscopic observations. We would like to thank the instrument specialists and telescope operators who were tremendously helpful in making sure these evenings went smoothly - Jim De Veny, Hal Halbedel, Heidi Schweiker, Doug Williams, Eugene McDougall, Karen Loomis, Camron Hastings, and Russet McMillan. N.A.M. would like to thank the NRAO pre-doctoral program for support of this research.

REFERENCES

Abell, G.O. 1958, ApJS, 3, 211

Abell, G.O., Corwin, H.G., and Olowin, R.P. 1989, ApJS, 70, 1

Becker, R.H., White, R.L., and Helfand, D.J. 1995, ApJ, 450, 559

Butcher, H., and Oemler, A. 1978, ApJ, 219, 18

Carilli, C.L., Miller, N.A., Poggianti, B.M., Yun, M.S., and Owen, F.N. 2001, in preparation

Condon, J.J. 1992, ARA&A, 30, 575

Condon, J.J., Cotton, W.D., Greisen, E.W., Yin, Q.F., Perley, R.A., Taylor, G.B., and Broderick, J.J. 1998, AJ, 115, 1693

Deutsch, E.W. 1999, AJ, 118, 188

Fanaroff, B.L., and Riley, J.M. 1974, MNRAS, 167, 31P

Fanti, R. 1984, in *Clusters and Groups of Galaxies* (Boston:Reidel), 185

Gregory, P.C., and Condon, J.J 1991, ApJS, 75, 1011

Gunn, J.E., and Oke, J.B. 1975, ApJ, 195, 225

Haarsma, D.B., Partridge, R.B., Windhorst, R.A., and Richards, E.A. 2000, ApJ, 544, 641

Haynes, M.P., Giovanelli, R., and Chincarini, G.L. 1984, ARA&A, 22, 445

Helou, G., Soifer, B.T., Rowan-Robinson, M. 1985, ApJ, 298, L7

Kennicutt, R.C., and Kent, S. M. 1983, AJ, 88, 1094

Kennicutt, R.C., Bothun, G.D., and Schommer, R.A. 1984, AJ, 89, 1279

Laing, R.A., Riley, J.M., and Longair, M.S. 1983, MNRAS, 204, 151 (3C Catalog)

Ledlow, M.J., and Owen, F.N. 1995a, AJ, 109, 853

Ledlow, M.J., and Owen, F.N. 1995b, AJ, 110, 1959

Ledlow, M.J., and Owen, F.N. 1996, AJ, 112, 9

Miller, N.A., and Owen, F.N. 2001, AJ, accepted

Owen, F.N., and Laing, R.A. 1989, MNRAS, 238, 357

Reid, I.N., Brewer, C., Brucato, R.J., McKinley, W.R., Maury, A., Mendenhall, D., Mould, J.R., Mueller, J., Neugebauer, G., Phinney, J., Sargent, W.L.W., Schombert, J., and Thicksten, R. 1991, PASP, 103, 661

Saunders, W., Sutherland, W.J., Maddox, S.J., Keeble, O., Oliver, S.J., Rowan- Robinson, M., McMahon, R.G., Efstathiou, G.P., Tadros, H., White, S.D.M., Frenk, C.S., Carramiñana, A., and Hawkins, M.R.S. 2000, MNRAS, in submission

Sijbring, D. 1993, PhD Thesis.

Struble, M.F., and Rood, H.J. 1999, ApJS, 125, 35

Tonry, J., and Davis, M. 1979, AJ, 84, 1511

Zhao, J.H., Burns, J.O., and Owen, F.N. 1989, AJ, 98, 64

This preprint was prepared with the AAS LaTeX macros v5.0.

Fig. 1.— Extended radio galaxies added to the sample (see Table 2). The NVSS positions of these galaxies were formally outside the search radius for their parent clusters, yet they were included as possible cluster radio galaxies on the basis of their morphologies. The optical images are all taken from the POSS II, and source of the overlaid contors is given for each plot. The base contour level for the NVSS is 450μJy, with contours at 2, 5, 10, 20, 40, 80, 160, and 360. For FIRST, the base contour level is 150μJy with contours at 5, 10, 20, 40, 80, 160, and 320. (a) Page one, top left - 022259+430042, NVSS contours. This source appears to exist in its own subpeak within the greater extended emission of 3C66B; (b) Page one, top right - 022308+412211, 022311+412204, NVSS contours. Each of these sources were accepted as radio galaxies; (c) Page one, bottom left - 025654+164844, NVSS contours. (d-e) Page two, top left and top right - 125635+281628, NVSS contours and FIRST contours, respectively. Rejected as the FIRST data show this is likely a background source; (f-g) Page two, bottom left and bottom right - 125818+290739, NVSS contours and FIRST contours, respectively. (h-i) Page three, top left and top right - 161829+295859, NVSS contours and FIRST contours, respectively. (j-k) Page three, bottom left and bottom right - 162505+394529, NVSS contours and FIRST contours, respectively. (l-m) Page four, top left and top right - 162842+400725, NVSS contours and FIRST contours, respectively. On the basis of the NVSS image, both of these galaxies were accepted. The emission is resolved out by FIRST. (n) Page four, bottom left - 233839+270040, NVSS contours. The galaxy can be seen to reside in its own subpeak within 3C465's extended emission. (o) Page four, bottom right - 234022+271104, NVSS contours.

Fig. 2.— q values derived from *xscanpi* vs. those derived from the IRAS Point Source Catalog (PSC). All galaxies on this plot were ones where the PSC reported a 90% confidence upper limit on the 100μm flux density. Filled circles represent cases where the cross scans yielded 100μm detections of such galaxies at greater than 3σ, whereas open circles remained upper limits. The solid line demonstrates that the two evaluations of q are consistent with one another.

Fig. 3.— Histogram of q values for all confirmed cluster radio galaxies. The shaded portion of the histogram represents those values for which the FIR flux, and hence the q value, is an upper limit. The strong peak at $q \sim 2.3$ results from the standard FIR-radio correlation, and consequently the majority of such galaxies are normal star-forming galaxies. Galaxies with $q \lesssim 2$ are normally AGN including LINERs and Seyferts, while those with $q \lesssim 1$ are powerful radio sources with elliptical hosts.

Table 1. Adopted Cluster Parameters

Cluster	Richness	RA	Dec	z	σ [km s^{-1}]	m_{zero}	A_R
A262	0	01:52:48	36:08:00	0.0163	588	29.99	0.13
A347	0	02:25:48	41:52:00	0.0184	777	30.10	0.11
A397	0	02:57:00	15:57:00	0.0327	566	30.10	0.22
A400	1	02:57:36	06:01:00	0.0244	663	30.10	0.17
A426	2	03:19:48	41:30:42	0.0179	1324	30.10	0.30
A539	1	05:16:36	06:27:00	0.0284	629	30.10	0.28
A569	0	07:09:18	48:37:00	0.0201	327	30.10	0.18
A634	0	08:14:36	58:02:00	0.0265	391	30.10	0.05
A779	0	09:19:51	33:46:17	0.0229	339	29.10[a]	0.00
A1185	1	11:10:48	28:40:00	0.0325	753	28.99[a]	0.00
A1267	0	11:27:54	26:51:00	0.0329	190	30.10	0.00
A1367	2	11:44:30	19:50:00	0.0220	879	29.73	0.00
A1656	2	12:59:48	27:58:00	0.0231	1008	30.18	0.03
A2162	0	16:12:30	29:32:00	0.0322	365	30.24	0.04
A2197	1	16:28:12	40:54:00	0.0308	593	30.49	0.00
A2199	2	16:28:36	39:31:00	0.0299	733	30.49	0.00
A2634	1	23:38:18	27:01:00	0.0310	1119	30.46	0.10
A2666	0	23:50:54	27:08:00	0.0272	518	30.46	0.07

[a] Digitized POSS II images not available for this cluster at the time of this writing. POSS I images have been used instead.

Note. — Column legend — (1) ACO cluster designation; (2) ACO richness class; (3-4) Adopted cluster center position, in J2000 coordinates; (5) Adopted cluster redshift; (6) Adopted cluster velocity dispersion, from Struble & Rood; (7) Zero point magnitude assumed for POSS II photometry of the cluster; (8) Average extinction assumed for POSS II photometry.

Table 2. Extended Radio Sources

Source	Cluster	Separation	$S_{1.4GHz}$	FIRST?	Accept?	Other Name
022259+430042[a]	A347	>99.9	<8577.	N	Y	UGC01837
022308+412211[b]	A347	31.5	<20.5	N	Y	UGC01840
022311+412204[b]	A347	49.4	<20.5	N	Y	UGC01840
025654+164844[a]	A397	50.1	<18.9	N	Y	—
025742+060128	A400	71.0	5836.	N	Y	3C75[c]
125635+281628	A1656	41.0	201.5	Y	N	—
125818+290739	A1656	73.9	8.6	Y	N[d]	—
125923+275441	A1656	25.3	445.6	Y	Y	NGC4869[e]
161236+292904	A2162	29.2	113.4	Y	Y	NGC6086[c]
161829+295859	A2162	54.0	144.2	Y	Y	—
162505+394529[a]	A2199	61.6	<38.0	Y	Y	—
162842+400725[a]	A2199	25.4	8.3	N	Y	—
233829+270155	A2634	26.7	7657.	N	Y	3C465[c]
233839+270040[a]	A2634	92.0	<7657.	N	Y	IC5342
234022+271104	A2634	39.2	62.5	N	Y	—

[a] Nearby stronger radio source. Accepted on account of radio morphology in contour image.

[b] Pair of galaxies associated with one radio source. The contour images suggests both are radio sources.

[c] See, e.g., Ledlow & Owen (1995a)

[d] Elliptical galaxy with weak Hα emission; FIRST image suggests radio emission associated with the galaxy is mainly from a background source.

[e] See, e.g., Sijbring (1993)

Note. — Column legend — (1) Source name from J2000 coordinates; (2) ACO cluster in which radio galaxy appears; (3) Separation between optical position and radio position as specified in the NVSS catalog; (4) Radio flux at 1.4GHz, determined directly from the NVSS image. If the radio source lies within a stronger extended source, an upper limit is indicated; (5) Indication of whether a FIRST image of the source is currently available; (6) Indication of whether the source is accepted in the list of cluster radio galaxy candidates, based on the FIRST image. If no FIRST image is available and only the NVSS image is used, the source is accepted. See Figure 1; (7) Common name of the radio galaxy, and reference where applicable.

Table 3. Spectroscopy Observing Runs

Dates	Observatory	Grating	Blaze	Dispersion	Slit Width	Wavelength Range
12/8/98, 12/24/98	APO	Med-B	4861	3.18	$2''$	3850 - 5275
		Med-R	6563	3.55	$2''$	5250 - 7250
1/9/99 - 1/11/99	APO	Med-B	4861	3.18	$2''$	3825 - 5250
		Med-R	6563	3.53	$2''$	5275 - 7275
4/9/99 - 4/11/99	APO	Med-B	4861	3.18	$2''$	3750 - 5250
		Med-R	6563	3.54	$2''$	5300 - 7300
5/8/99 - 5/12/99	KPNO	09	4000	2.40	$2''$	3700 - 8000
12/4/99 - 12/10/99	KPNO	09	4000	2.43	$2''$	3600 - 7900

Note. — Column legend — (1) Calendar dates of scheduled observations. Note that APO time is scheduled in half-night blocks so each date corresponds to half a night of scheduled observing; (2) Observatory where observations were performed. APO signifies observations at the Apache Point Observatory with the 3.5-meter telescope and the Double Imaging Spectrograph, and KPNO signifies observations made at the Kitt Peak National Observatory on the 2.1-meter telescope with the GoldCam spectrograph; (3) Choice of gratings. Note that for APO, the incident light is split into a blue and a red spectrum by a dichroic. The gratings and detector characteristics differ for the two systems; (4) Blaze angle of grating, in Angstroms. APO's gratings are believed to have blaze angles corresponding to the Balmer lines; (5) Resolution of resulting spectra, in Å $pixel^{-1}$; (6) Slit width, in arcseconds; (7) Wavelength range of resulting spectra, in Angstroms. Note that for the APO red spectra, the range extends beyond that quoted but we have truncated it in the table as our sensitivity function is fit over this this range. In the case of the KPNO spectra, the chip size allows a greater wavelength range but instrument focus degrades at the extremes.

Table 4. Measured Radio Galaxy Velocities

Source	Observing Run	z	Error	Emission Lines
014736+373723	KPNO-2	0.0744	0.0002	(Hα, [NII])
015040+372308	KPNO-2	0.0737	0.0002	—
015129+360356	KPNO-2	0.0178	0.0001	Hα, Hβ, [NII], [SII]
015240+361016	KPNO-2	0.0186	0.0002	(Hα, [NII])
015246+360907	KPNO-2	0.0171	0.0004	(Hα, [NII])
015254+360311	KPNO-2	0.0206	0.0001	Hα, Hβ, [NII]
015417+341855	KPNO-2	0.0859	0.0002	—
015628+364807	KPNO-2	0.0198	0.0002	Hα, Hβ, [NII], [SII]
015644+362304	KPNO-2	0.0156	0.0002	—
015742+355456	KPNO-2	0.0169	0.0002	([NII])
015750+362034	KPNO-2	0.0156	0.0002	Hα, [NII], [SII]
015855+364029	KPNO-2	0.0166	0.0002	—
015958+372331	KPNO-2	0.0489	0.0002	—
021359+412029	KPNO-2	0.0874	0.0002	Hα, [NII], [SII]
021914+414258	KPNO-2	0.0196	0.0001	Hα - Hγ, [NII], [OI], [OII], [OIII], [SII]
022004+411628	KPNO-2	0.0195	0.0001	Hα - Hγ, [NII], [OII], [OIII], [SII]
022259+430042	KPNO-2	0.0221	0.0002	—
022307+412223	KPNO-2	0.0171	0.0001	Hα, Hβ, [NII], [SII]
022308+412211	KPNO-2	0.0177	0.0001	Hα, [NII], [SII]
022311+412204	KPNO-2	0.0185	0.0002	—
022429+405212	KPNO-2	0.0434	0.0002	(Hα, [NII])
022447+420125	KPNO-2	0.0203	0.0002	Hα, [NII], [SII]
022453+431929	KPNO-2	0.0177	0.0003	Hα, [NII], [OII], [SII]
022516+420522	KPNO-2	0.0156	0.0003	—
022605+420837	KPNO-2	0.0186	0.0003	Hα, [NII]
022613+394550	KPNO-2	0.0755	0.0003	Hα, [NII], [SII]
022653+414124	KPNO-2	0.0144	0.0001	Hα, [NII], [SII]
022655+420058	KPNO-2	0.0153	0.0002	Hα, [NII], [SII]
022731+415552	KPNO-2	0.0194	0.0002	Hα, [NII], [SII]
022735+415840	KPNO-2	0.0189	0.0001	Hα, Hβ, [NII], [SII]
022737+420027	KPNO-2	0.0189	0.0001	Hα - Hγ, [NII], [OII], [OIII], [SII]
022901+424143	KPNO-2	0.0215	0.0002	Hα, [NII], [SII]
022924+402546	KPNO-2	0.0162	0.0002	Hα, [NII], [SII]
023113+432129	KPNO-2	0.0221	0.0003	Hα, [NII], [SII]
023114+402325	KPNO-2	0.0192	0.0002	Hα, [NII], [SII]
023324+425231	KPNO-2	0.0432	0.0002	Hα, [NII], [SII]
023329+401337	KPNO-2	0.0560	0.0002	(Hα, [NII])
023344+400545	KPNO-2	0.0360	0.0003	—

Table 4—Continued

Source	Observing Run	z	Error	Emission Lines
023453+410706	KPNO-2	0.0630	0.0002	—
023525+405209	KPNO-2	0.0197	0.0002	([NII])
023806+414722	KPNO-2	0.0181	0.0003	—
025246+063919	APO-1	0.0627	0.0002	—
025302+151141	KPNO-2	0.0329	0.0001	Hα, [NII], [SII]
025338+060338	APO-1	0.0256	0.0002	Hα, Hβ, [NII], [OIII], [SII]
025402+145828n	KPNO-2	0.0323	0.0002	[c]
025402+145828s	KPNO-2	0.0316	0.0001	Hα - Hγ, [NII], [OII], [OIII], [SII][c]
025405+145409	KPNO-2	0.1063	0.0003	—
025411+154346	KPNO-2	0.0758	0.0002	—
025430+145050	KPNO-2	0.1065	0.0002	—
025435+051506	APO-1	0.0247	0.0002	Hα, Hβ, [NII], [OIII], [SII]
025528+154832	KPNO-2	0.0365	0.0001	Hα, Hβ, [NII], [SII]
025614+170821	KPNO-2	0.0335	0.0001	Hα, Hβ, [NII], [OII], [OIII], [SII]
025626+065623	APO-1	0.1167	0.0003	—
025628+160029	KPNO-2	0.0301	0.0001	(Hα, [NII])
025643+072000	KPNO-2	0.0276	0.0002	([NII])
025654+164844	KPNO-2	0.0331	0.0001	Hα, [NII], [SII]
025705+155859	KPNO-2	0.0315	0.0001	—
025716+154302	KPNO-2	0.0779	0.0003	(Hα, [NII])
025726+152817	KPNO-2	0.0335	0.0001	Hα, Hβ, [NII], [SII]
025757+051700	APO-1	0.0165	0.0002	Hα - Hϵ, [NII], [OI], [OII], [OIII], [SII]
025829+061220	APO-1	0.0225	0.0002	—
025850+042314	APO-1	0.0341	0.0002	Hα, Hβ, [NII]
025916+060800	KPNO-2	0.0275	0.0001	Hα, [NII], [SII]
025919+160438	KPNO-2	0.0683	0.0001	Hα, [NII], [SII]
025936+060546	APO-1	0.0342	0.0002	Hα - Hγ, [NII], [OIII], [SII]
030000+150934	KPNO-2	0.0724	0.0001	Hα, Hβ, [NII], [OII], [SII]
030211+155538	KPNO-2	0.0170	0.0001	Hα - Hγ, [NII], [OII], [OIII], [SII]
030656+413724	KPNO-2	0.0494	0.0003	(Hα, [NII])
030748+412231	KPNO-2	0.0221	0.0002	([NII])
030813+422631	KPNO-2	0.0655	0.0002	—
031008+424948	APO-1	0.0307	0.0002	—
031014+424947	APO-1	0.0289	0.0002	—
031156+414138	KPNO-2	0.0316	0.0001	Hα, Hβ, [NII], [SII]
031358+411524	KPNO-2	0.0294	0.0003	([NII], [SII])
031410+403718	KPNO-2	0.0287	0.0001	Hα, Hβ, [NII], [OII], [SII]
031432+424616	APO-1	0.0303	0.0002	—

Table 4—Continued

Source	Observing Run	z	Error	Emission Lines
031647+400013	KPNO-2	0.0142	0.0003	—
031751+412703	KPNO-2	0.0150	0.0002	([NII], [SII])
032012+412200	KPNO-2	0.0072	0.0002	—
032031+430651	APO-2	0.0524	0.0002	—
032038+430444	KPNO-2	0.0517	0.0003	—
032051+413602	APO-1	0.0177	0.0002	—
032140+412136	KPNO-2	0.0222	0.0002	—
032326+390635	KPNO-2	0.0411	0.0002	Hα, [NII], [OI], [OII], [OIII], [SII]
032423+404719	KPNO-2	0.0130	0.0002	Hα, [NII], [OI], [OII], [OIII], [SII]
032503+405829	KPNO-2	0.0466	0.0001	Hα, [NII], [SII]
032526+403210	KPNO-2	0.0121	0.0002	Hα, Hβ, [OIII]
032601+420128	APO-1	0.0308	0.0003	[a]
032635+414142	KPNO-2	0.0142	0.0001	Hα, [NII], [OII], [SII]
032755+395949	KPNO-2	0.0251	0.0002	—
032821+431041	KPNO-2	0.0318	0.0002	Hα, [NII], [OII], [SII]
051120+062151	KPNO-2	0.1042	0.0002	—
051324+073135	KPNO-2	0.0302	0.0002	Hα, Hβ, [NII], [OII], [OIII], [SII]
051330+072506	KPNO-2	0.0289	0.0002	Hα, [NII], [OIII], [SII]
051710+065537	KPNO-2	0.0283	0.0004	(Hα, [NII])
051831+045748	KPNO-2	0.0694	0.0003	Hα, [NII], [OII], [SII]
051913+055240	KPNO-2	0.0307	0.0001	Hα, [NII], [SII]
051951+052959	KPNO-2	0.0292	0.0002	(Hα, [NII])
052146+064118	KPNO-2	0.0300	0.0001	—
052150+064036	KPNO-2	0.0317	0.0003	Hα, [NII]
065835+473852	KPNO-2	0.0912	0.0003	—
065904+490235	KPNO-2	0.0919	0.0002	—
070153+473957	KPNO-2	0.0536	0.0002	—
070158+464841	KPNO-2	0.0263	0.0001	Hα - Hγ, [NII], [OII], [OIII], [SII]
070206+485918	KPNO-2	0.0649	0.0002	—
070209+471048	KPNO-2	0.0587	0.0002	—
070233+503526	KPNO-2	0.0210	0.0002	(Hα, [NII])
070303+492529	KPNO-2	0.0189	0.0003	(Hα, [NII])
070542+503452	KPNO-2	0.0197	0.0002	([NII], [SII])
070719+482105	KPNO-2	0.0419	0.0001	Hα, [NII], [SII]
070752+482451	KPNO-2	0.0184	0.0001	Hα, [NII], [SII]
070811+504055	KPNO-2	0.0201	0.0002	([NII])
070834+503752	KPNO-2	0.0205	0.0001	Hα, Hβ, [NII], [OII], [OIII], [SII]
070908+483656	KPNO-2	0.0197	0.0001	([NII])

Table 4—Continued

Source	Observing Run	z	Error	Emission Lines
070916+494914	KPNO-2	0.0156	0.0001	Hα, Hβ, [NII], [OIII], [SII]
070918+495216	KPNO-2	0.0165	0.0002	Hα, Hβ, [NII], [OII], [SII]
070923+483808	KPNO-2	0.0206	0.0001	—
070934+501056	KPNO-2	0.0196	0.0002	—
070938+472606	KPNO-2	0.0607	0.0002	—
071034+500708	KPNO-2	0.0214	0.0002	—
071142+495144	KPNO-2	0.0206	0.0002	—
071153+501238	KPNO-2	0.0606	0.0002	—
071244+500343	KPNO-2	0.0184	0.0002	—
071652+495229	KPNO-2	0.0210	0.0002	Hα, [NII], [OIII], [SII]
072033+490518	KPNO-2	0.0281	0.0001	Hα, Hβ, [NII], [SII]
072219+491732	KPNO-2	0.0206	0.0002	Hα, [NII], [SII]
080845+563531	KPNO-2	0.0272	0.0003	Hα, [NII]
080932+584423	KPNO-2	0.0689	0.0002	—
080940+573127	KPNO-2	0.0255	0.0003	—
080940+575302	KPNO-2	0.0890	0.0005	—
080941+584512	KPNO-2	0.0697	0.0002	—
080953+575445	KPNO-2	0.0266	0.0001	([NII])
081217+583351	KPNO-2	0.0269	0.0001	Hα, Hβ, [NII], [OI], [OII], [OIII], [SII]
081251+575516	KPNO-2	0.0267	0.0001	Hα, Hβ, [NII], [OIII], [SII]
081545+581914	KPNO-2	0.0271	0.0002	—
082009+564334	KPNO-2	0.0807	0.0001	Hα, Hβ, [NII], [SII]
082203+571829	KPNO-2	0.0267	0.0003	Hα, [NII]
091525+331605	APO-2	0.0627	0.0002	Hα, Hβ, [NII], [OII], [SII]
091833+342040	APO-2	0.0459	0.0002	Hα, Hβ, [NII], [OI], [OII], [SII]
091924+333727	KPNO-2	0.0213	0.0001	—
091941+334418	KPNO-2	0.0208	0.0003	—
091947+334457	KPNO-2	0.0232	0.0002	—
110508+283657	APO-2	0.0346	0.0002	Hα, Hβ, [NII], [OII], [OIII], [SII]
110554+284800	APO-2	0.0331	0.0003	Hα, [NII], [OII]
110709+283532	APO-2	0.0338	0.0003	Hα, [NII], [OII], [SII]
110747+281034	APO-2	0.0650	0.0002	Hα - Hγ, [NII], [OII], [SII]
110823+291427	APO-2	0.2126	0.0002	—
110830+295013	KPNO-2	0.0355	0.0001	Hα, Hβ, [NII], [OII], [OIII], [SII]
110933+283740	KPNO-2	0.0381	0.0001	Hα, [NII], [OIII], [SII]
111039+271352	KPNO-1	0.0446	0.0001	Hα - Hγ, [NII], [OI], [OII], [OIII], [SII]
111056+283237	KPNO-2	0.0321	0.0001	—
111100+292011	APO-2	0.0293	0.0002	Hα, Hβ, [NII], [OII], [OIII], [SII]

Table 4—Continued

Source	Observing Run	z	Error	Emission Lines
111113+284243	KPNO-2	0.0289	0.0003	Hα - Hγ, [NII], [OII], [OIII], [SII]
111113+284147	KPNO-2	0.0287	0.0001	Hα, [NII], [OI], [OII], [SII]
111119+284051	KPNO-2	0.0294	0.0002	([NII])
111149+294021	KPNO-2	0.0563	0.0002	—
111202+275054	KPNO-1	0.0475	0.0004	Hα, [NII], [OII], [OIII], [SII]
111204+273401	KPNO-2	0.0366	0.0001	—
111310+274906	KPNO-2	0.0314	0.0001	([NII])
111311+280043	KPNO-2	0.0321	0.0002	Hα, [NII], [OII], [OIII], [SII]
111319+294839	APO-2	0.0451	0.0001	—
112144+262642	KPNO-1	0.0510	0.0001	Hα, [NII], [SII]
112330+270608	APO-2	0.0687	0.0002	Hα - Hγ, [NII], [OII], [SII]
112411+270050	APO-2	0.0330	0.0002	—
112412+272718	APO-2	0.1018	0.0001	—
112424+274244	APO-2	0.0324	0.0002	Hα, Hβ, [NII], [OI], [OII], [OIII], [SII]
112532+263902	APO-2	0.0872	0.0002	—
112555+264120	KPNO-1	0.0878	0.0001	—
112616+275201	APO-2	0.0239	0.0002	Hα - Hδ, [NII], [OIII], [SII]
112815+261402	APO-2	0.1068	0.0004	Hα, [NII], [OII], [SII]
112825+272719	KPNO-1	0.0335	0.0001	Hα - Hγ, [NII], [OI], [OII], [OIII], [SII]
112839+265713	APO-2	0.0524	0.0003	Hα, Hβ, [NII], [OI], [OII], [OIII], [SII]
112857+274746	APO-2	0.0682	0.0002	Hα, Hβ, [NII], [OII], [SII]
112912+273312	APO-2	0.0732	0.0001	—
113013+262343	KPNO-1	0.0574	0.0002	—
113028+254857	KPNO-1	0.0336	0.0002	Hα, Hβ, [NII], [OI], [OII], [OIII], [SII]
113049+252436	APO-2	0.1444	0.0002	[b]
113053+261927	APO-2	0.0332	0.0003	Hα, [NII], [OII]
113109+261333	APO-2	0.0334	0.0002	Hα, [OI], [OII], [OIII], [NII], [SII]
113146+262831	KPNO-1	0.0328	0.0004	(Hα, [NII])
113157+265557	APO-2	0.1005	0.0004	—
113402+263223	APO-2	0.0771	0.0001	—
113654+195815	KPNO-1	0.0206	0.0001	Hα - Hδ, [NII], [OII], [OIII], [SII]
114006+181322	KPNO-1	0.1242	0.0002	—
114159+184353	KPNO-1	0.0705	0.0002	(Hα, [NII])
114225+200708	KPNO-1	0.0201	0.0002	Hα, Hβ, [NII], [SII]
114256+195755	KPNO-1	0.0245	0.0001	Hα, Hβ, [NII], [OII], [OIII], [SII]
114313+200016	KPNO-1	0.0234	0.0002	Hα - Hδ, [NII], [OII], [OIII], [SII]
114349+195811	KPNO-1	0.0221	0.0002	Hα, Hβ, [NII], [OII], [OIII], [SII]
114358+204822	KPNO-1	0.0213	0.0002	Hα, Hβ, [NII], [SII]

Table 4—Continued

Source	Observing Run	z	Error	Emission Lines
114449+194741	KPNO-1	0.0190	0.0003	Hα, [NII], [SII]
114455+194634	KPNO-1	0.0276	0.0002	Hα, Hβ, [NII], [OI], [OII], [OIII], [SII]
114504+195824	KPNO-1	0.0171	0.0002	(Hα, [NII], [SII])
114549+203742	KPNO-1	0.0235	0.0002	Hα - Hγ, [NII], [OII], [OIII], [SII]
114612+202329	KPNO-1	0.0232	0.0002	Hα, [NII], [OI], [OIII], [SII]
114647+211616	KPNO-1	0.0223	0.0002	Hα, Hβ, [NII]
115052+211014	KPNO-1	0.0259	0.0002	Hα, Hβ, [NII], [OIII], [SII]
115201+203931	KPNO-1	0.0203	0.0002	Hα, Hβ, [NII], [OII], [OIII], [SII]
115243+203752	KPNO-1	0.0226	0.0002	—
125254+282214	KPNO-1	0.0237	0.0002	Hα, Hβ, [NII], [OII], [SII]
125725+272415	KPNO-1	0.0162	0.0001	Hα - Hγ, [NII], [OII], [OIII], [SII]
125731+263042	KPNO-1	0.0241	0.0002	Hα, Hβ, [NII], [OIII], [SII]
125758+280339	KPNO-1	0.0273	0.0001	Hα, Hβ, [NII], [SII]
125806+281433	KPNO-1	0.0245	0.0001	Hα, Hβ, [NII], [OII], [OIII], [SII]
125818+290739	KPNO-1	0.0266	0.0002	(Hα, [NII])
125835+273545	KPNO-1	0.0258	0.0003	(Hα, [NII])
125837+271033	KPNO-1	0.0257	0.0001	Hα - Hγ, [NII], [OIII], [SII]
130034+273814	KPNO-1	0.0251	0.0002	Hα, Hβ, [NII], [OII], [OIII], [SII]
130038+280325	KPNO-1	0.0258	0.0001	Hα, Hβ, [NII], [OII], [OIII], [SII]
130041+283109	KPNO-1	0.0297	0.0001	Hα - Hγ, [NII], [OI], [OII], [OIII], [SII]
130056+274725	KPNO-1	0.0270	0.0002	(Hα, [NII])
130125+291835	KPNO-1	0.0240	0.0002	[c]
130125+291848	KPNO-1	0.0235	0.0002	Hα - Hγ, [NII], [OII], [OIII], [SII][c]
130134+290749	KPNO-1	0.0246	0.0002	—
130158+280020	KPNO-1	0.0260	0.0002	—
130317+271956	KPNO-1	0.0358	0.0002	Hα - Hγ, [NII], [OII], [OIII], [SII]
130617+290346	KPNO-1	0.0236	0.0002	(Hα, [NII])
130636+275221	KPNO-1	0.0210	0.0002	Hα, Hβ, [NII], [SII]
160632+292756	KPNO-1	0.0917	0.0003	Hα, [NII], [SII]
160943+302709	KPNO-1	0.0309	0.0002	—
161027+302916	KPNO-1	0.1246	0.0003	—
161052+300203	KPNO-1	0.0994	0.0003	Hα, [NII], [OIII]
161145+294523	KPNO-1	0.0516	0.0003	—
161145+294452	KPNO-1	0.0509	0.0002	—
161218+282545	KPNO-1	0.0532	0.0003	—
161243+295403	KPNO-1	0.0533	0.0002	—
161257+304614	KPNO-1	0.0498	0.0002	—
161305+305406	KPNO-1	0.0508	0.0002	—

Table 4—Continued

Source	Observing Run	z	Error	Emission Lines
161319+305436	KPNO-1	0.1529	0.0002	Hα - Hγ, [NII], [OII], [OIII]
161330+290835	KPNO-1	0.0785	0.0002	—
161428+281730	KPNO-1	0.1069	0.0002	—
161829+295859	KPNO-1	0.1340	0.0004	—
162056+395139	APO-3	0.0288	0.0001	Hα - Hγ, [NII], [OII], [OIII], [SII]
162122+404836	KPNO-1	0.0303	0.0005	(Hα, [NII])
162142+403527	APO-3	0.0312	0.0002	Hα, Hβ, [NII], [OII], [OIII], [SII]
162254+402946	APO-3	0.0310	0.0002	Hα - Hγ, [NII], [OI], [OII], [OIII], [SII]
162317+395510	APO-3	0.0322	0.0002	([NII], [OII], [SII])
162418+391240	APO-3	0.0300	0.0002	([NII], [OII])
162437+390739	APO-3	0.0349	0.0002	Hα, Hβ, [NII], [OII], [OIII], [SII]
162446+391050	APO-3	0.1015	0.0002	—
162524+384822	APO-3	0.0315	0.0002	Hα - Hγ, [NII], [OI], [OII], [SII]
162531+400813	APO-3	0.0328	0.0002	Hα, Hβ, [NII], [OII], [OIII], [SII]
162544+402831	APO-3	0.0317	0.0002	Hα, Hβ, [NII], [OII], [SII]
162550+402918	KPNO-1	0.0290	0.0003	—
162711+405423	APO-3	0.0318	0.0002	Hα, Hβ, [NII], [OII], [OIII], [SII]
162808+421659	APO-3	0.0455	0.0004	[OII], [OIII]
162840+400724	APO-3	0.0260	0.0002	Hα, Hβ, [NII]
162842+400725	APO-3	0.0337	0.0002	Hα, Hβ, [NII], [OII], [OIII], [SII]
162920+392543	APO-3	0.0277	0.0002	—
162951+394558	APO-3	0.0317	0.0001	—
163033+392302	KPNO-1	0.0305	0.0001	Hα, Hβ, [NII], [OI], [OII], [OIII], [SII]
163107+392547	APO-3	0.0636	0.0004	Hα, [NII]
163350+391546	KPNO-1	0.0318	0.0001	Hα, Hβ, [NII], [OII], [OIII], [SII]
163452+401140	APO-3	0.0306	0.0002	Hα, Hβ, [NII], [OIII], [SII]
233549+261323	KPNO-2	0.1636	0.0004	—
233626+275607	KPNO-2	0.0296	0.0002	Hα, [NII], [SII]
233839+270040	KPNO-2	0.0312	0.0001	—
233915+273349	KPNO-2	0.0660	0.0001	Hα, [NII], [SII]
234015+265838	KPNO-2	0.1772	0.0006	—
234047+265007	KPNO-2	0.0392	0.0001	—
234238+270528	KPNO-2	0.0251	0.0001	Hα, Hβ, [NII], [OII], [SII]
234250+273258	KPNO-2	0.0237	0.0002	Hα, Hβ, [NII], [OI], [OIII], [SII]
234401+274254	KPNO-2	0.0248	0.0002	Hα, [NII], [OIII], [SII]
234437+274833	KPNO-2	0.0573	0.0001	(Hα, [NII])
234507+281219	KPNO-2	0.0241	0.0001	([NII])
234532+272138	KPNO-2	0.0260	0.0002	(Hα, [NII])

Table 4—Continued

Source	Observing Run	z	Error	Emission Lines
234547+272020	KPNO-2	0.0307	0.0001	Hα, Hβ, [NII], [OIII], [SII]
234652+265615	KPNO-2	0.0731	0.0005	—
234734+282606	KPNO-2	0.0301	0.0001	Hα, [NII], [SII]
234828+270249	KPNO-2	0.0661	0.0003	(Hα, [NII])
235257+272304	KPNO-2	0.0517	0.0001	Hα, Hβ, [NII], [SII]
235508+275908	KPNO-2	0.0303	0.0002	Hα, Hβ, [NII], [OI], [OIII], [SII]
235550+265054	KPNO-2	0.0266	0.0003	([NII])

[a] Due to mis-alignment of the slit, this is an off-nuclear spectrum. Nuclear emission lines may be present.

[b] Outside radial extent of sample; included as serendipitous finding of an extended radio galaxy.

[c] This appears to be an interacting system, with the radio emission centered on emission line object.

Note. — Column legend — (1) Source name, from J2000 coordinates; (2) Observing run during which spectrum was collected. 'APO' represents data collected at Apache Point Observatory, with the attached number indicating the observing run (1 = December 1998, 2 = January 1999, 3 = April 1999). 'KPNO' represents data collected at Kitt Peak National Observatory, with the attached number indicating the observing run (1 = May 1999, 2 = December 1999); (3) Heliocentric redshift of galaxy; (4) Error in redshift measurement; (5) Where emission lines are present, the galaxy's redshift has been determined from them and the identified lines are indicated here. If no emission lines are present ('—'), the velocity has been determined via fourier cross correlation of the galaxy's absorption lines. In the event that emission lines are present but weak, the velocity has been determined via fourier cross correlation and identified lines are listed in parentheses.

Table 5. Cluster Radio Galaxy Data

Cluster	RA (J2000)	Dec (J2000)	z	m	$S_{1.4GHz}$ [mJy]	$S_{60\mu m}$ [Jy]	$S_{100\mu m}$ [Jy]	q	Common Name
A262	01:41:15.6	34:48:40.3	0.0170[a]	13.0	5.8	0.788	1.443	2.30	—
	01:44:35.5	37:41:46.1	0.0189[a]	12.7	18.9	1.878	4.595	2.22	NGC0662
	01:44:38.3	34:39:35.5	0.0189[a]	13.9	3.7	0.362	0.807	2.20	—
	01:46:22.7	36:27:35.7	0.0150[a]	12.3	3.4	0.750	2.048	2.60	NGC0668
	01:46:57.0	34:46:19.3	0.0140[a]	13.2	4.2	0.496	1.191	2.30	VV701
	01:50:41.1	33:44:25.8	0.0187[a]	14.1	4.0	0.548	1.017	2.31	MRK1008
	01:50:44.3	35:17:03.2	0.0138[a]	12.1	10.3	1.286	2.783	2.30	NGC0688
	01:51:29.3	36:03:56.5	0.0178	12.9	19.4	0.923	2.736	1.95	UGC01319
	01:52:39.7	36:10:15.7	0.0186	12.6	8.6	0.248	0.870	1.77	NGC0703
	01:52:45.9	36:37:06.2	0.0185[a]	12.0	13.5	1.485	3.840	2.28	UGC01347
	01:52:46.5	36:09:07.1	0.0171	11.7	66.8	0.440[d]	1.310[d]	1.09	NGC0708
	01:52:54.1	36:03:11.0	0.0206	12.6	36.1	1.439	3.256	1.81	NGC0710
	01:54:54.0	36:55:03.5	0.0188[a]	13.2	18.7	5.486	7.780	2.60	UGC01385
	01:56:27.8	36:48:07.3	0.0198	12.9	8.6	0.380[d]	0.444[e]	1.75	NGC0732
	01:56:37.9	34:10:37.9	0.0154[a]	12.4	4.3	0.442	1.450	2.31	NGC0735
	01:56:44.0	36:23:03.6	0.0156	13.1	3.0	0.096[e]	0.200[d]	1.70	UGC01415
	01:57:42.3	35:54:56.3	0.0169	11.7	35.2	3.361	11.400	2.28	NGC0753
	01:57:50.5	36:20:34.1	0.0156	12.0	15.6	0.737	2.076	1.93	NGC0759
	01:58:54.9	36:40:28.6	0.0166	12.5	3.7	0.623	2.503	2.57	IC0178
	01:59:05.0	36:15:29.3	0.0165[a]	12.7	3.8	0.734	1.518	2.48	UGC01460
	02:00:55.2	38:12:38.3	0.0138[a]	12.0	7.1	1.288	3.648	2.52	UGC01493
A347	02:13:59.9	41:52:36.5	0.0144[a]	13.4	15.5	3.001	3.043	2.37	—
	02:18:54.2	42:34:39.0	0.0183[a]	14.4	12.2	1.555	2.697	2.27	—
	02:19:13.8	41:42:58.4	0.0196	13.2	7.6	0.680[d]	1.470[d]	2.15	—
	02:20:04.0	41:16:28.2	0.0195	13.2	8.3	0.880[d]	1.670[d]	2.20	—
	02:21:23.6	42:52:32.6	0.0221[a]	12.9	19.8	2.704	5.205	2.32	—
	02:22:58.6	43:00:41.7	0.0221	12.2	<8577.[c]	0.080[e]	0.590[e]	-1.50	UGC01837
	02:23:08.1	41:22:10.8	0.0177	12.6	<20.5[c]	0.860[d]	1.750[d]	1.81	UGC01840
	02:23:11.4	41:22:04.5	0.0185	12.6	<20.5[c]	0.790[d]	1.560[d]	1.77	UGC01840
	02:23:11.8	42:59:29.2	0.0212[a]	11.5	8577.[b]	0.230[d]	0.810[d]	-1.26	3C66B
	02:24:44.4	42:37:20.9	0.0203[a]	12.4	2.8	0.108[e]	0.579[e]	2.01	UGC01859
	02:24:47.1	42:01:25.4	0.0203	13.6	4.9	0.630[d]	1.280[d]	2.30	—
	02:24:53.3	43:19:29.1	0.0177	12.6	14.3	0.132[e]	0.720[d]	1.40	—
	02:25:16.3	42:05:21.7	0.0156	12.0	8.1	0.410[d]	1.520[d]	2.03	NGC0906
	02:26:05.1	42:08:37.1	0.0186	12.1	21.5	1.340[d]	3.330[d]	2.03	NGC0914
	02:26:46.3	41:50:02.7	0.0191[a]	12.9	15.3	3.361	5.468	2.49	—
	02:26:53.2	41:41:24.4	0.0144	12.9	4.9	0.940[d]	1.390[d]	2.42	—

Table 5—Continued

Cluster	RA (J2000)	Dec (J2000)	z	m	$S_{1.4GHz}$ [mJy]	$S_{60\mu m}$ [Jy]	$S_{100\mu m}$ [Jy]	q	Common Name
	02:26:55.0	42:00:58.5	0.0153	13.6	4.1	0.180[d]	0.321[e]	1.81	—
	02:27:31.4	41:55:51.8	0.0194	13.1	10.4	3.030[d]	6.130[d]	2.52	—
	02:27:34.7	41:58:40.0	0.0189	12.6	24.1	4.720[d]	9.780[d]	2.48	NGC0923
	02:27:36.8	42:00:26.6	0.0189	13.0	4.7	3.310[d]	7.370[d]	3.06	MRK1176
	02:29:01.1	42:41:42.9	0.0215	13.9	3.2	1.080[d]	2.430[d]	2.74	—
	02:29:24.5	40:25:45.7	0.0162	14.0	3.5	0.105[e]	0.279[e]	1.72	—
	02:31:12.9	43:21:28.9	0.0221	13.6	9.8	0.460[d]	2.090[d]	2.09	—
	02:31:14.3	40:23:24.9	0.0192	12.8	9.7	1.070[d]	3.130[d]	2.31	UGC01988
	02:35:24.9	40:52:09.5	0.0197	11.9	24.6	1.700[d]	5.340[d]	2.12	NGC0980
	02:38:05.6	41:47:22.1	0.0181	12.6	8.0	0.930[d]	2.950[d]	2.35	UGC02111
A397	02:53:02.0	15:11:41.0	0.0329	15.2	3.5	0.420[d]	1.200[d]	2.34	—
	02:54:01.8	14:58:27.9	0.0323	13.2	49.5	7.680	10.310	2.31	UGC02369
	02:55:28.0	15:48:32.5	0.0365	15.6	2.8	0.072[e]	0.567[e]	1.96	—
	02:56:14.4	17:08:21.1	0.0335	14.8	3.7	0.690[d]	1.330[d]	2.45	—
	02:56:27.9	16:00:28.7	0.0301	14.1	24.5	0.200[d]	1.270[d]	1.39	—
	02:56:34.7	16:53:04.0	0.0326[a]	14.2	2.6	0.114[e]	0.768[e]	2.14	—
	02:56:53.8	16:48:43.7	0.0331	14.8	<18.9[c]	0.360[d]	0.756[e]	1.48	—
	02:57:04.6	15:58:59.3	0.0315	14.1	8.3	0.250[d]	2.260[d]	2.07	—
	02:57:25.7	15:28:17.5	0.0335	14.4	3.1	0.460[d]	0.468[e]	2.25	—
	02:58:35.6	16:05:16.2	0.0288[a]	14.5	4.4	0.660[d]	0.570[d]	2.24	—
	02:59:22.2	16:15:31.4	0.0354[a]	15.1	4.3	0.096[e]	0.990[d]	1.99	—
	02:59:58.5	16:35:00.9	0.0311[a]	14.9	5.8	1.159	1.753	2.44	—
A400	02:53:31.3	06:28:24.0	0.0251[a]	13.9	6.1	0.476	2.382	2.30	—
	02:53:37.7	06:03:38.2	0.0256	14.7	3.1	0.430[d]	1.194[e]	2.40	—
	02:53:58.8	05:59:15.4	0.0264[a]	14.1	3.0	0.520[d]	2.292[e]	2.61	UGC02372
	02:54:03.6	06:15:26.7	0.0254[a]	13.9	2.9	0.168[e]	2.184[e]	2.48	UGC02375
	02:54:34.6	05:15:05.6	0.0247	14.5	4.3	0.950[d]	2.040[d]	2.55	—
	02:56:17.7	04:31:45.4	0.0276[a]	14.4	3.7	0.132[e]	1.440[d]	2.21	UGC02414
	02:56:28.4	04:36:37.4	0.0271[a]	14.1	3.3	0.400[d]	1.510[d]	2.41	—
	02:56:42.1	05:59:36.4	0.0232[a]	15.0	5.1	0.183[e]	2.520[e]	2.29	—
	02:56:43.2	07:19:59.7	0.0276	13.2	4.6	0.713	2.375	2.49	UGC02419
	02:56:45.9	06:03:17.2	0.0261[a]	14.9	4.0	0.220[d]	2.844[e]	2.46	—
	02:56:56.7	06:12:19.3	0.0213[a]	13.9	6.8	1.118	2.136	2.39	—
	02:57:41.7	06:01:27.7	0.0230[f]	12.7	5836.[c]	0.500[d]	0.790[d]	-0.92	3C75
	02:58:28.6	06:12:20.3	0.0225	14.6	5.9	0.150[d]	1.173[e]	1.95	—
	02:58:29.8	06:18:21.9	0.0224[a]	13.6	12.5	1.285	3.396	2.26	UGC02444
	02:59:16.2	06:07:59.6	0.0275	14.1	5.2	0.400[d]	1.270[d]	2.17	—

Table 5—Continued

Cluster	RA (J2000)	Dec (J2000)	z	m	$S_{1.4GHz}$ [mJy]	$S_{60\mu m}$ [Jy]	$S_{100\mu m}$ [Jy]	q	Common Name
A426	03:07:47.9	41:22:31.4	0.0221	13.3	6.0	0.320[d]	2.085[e]	2.21	—
	03:10:08.5	42:49:48.4	0.0307	12.9	1205.4[b]	0.320[d]	1.130[d]	-0.26	—
	03:10:13.0	40:45:56.3	0.0100[a]	12.5	12.7	1.980[d]	4.630[d]	2.41	IC0292
	03:13:10.3	42:59:50.8	0.0301[a]	13.9	4.2	0.760[d]	2.740[d]	2.58	—
	03:13:57.7	41:15:24.2	0.0294	13.0	41.3	0.400[d]	1.260[d]	1.27	—
	03:14:09.9	40:37:18.5	0.0287	14.2[g]	7.6	1.300[d]	8.090[d]	2.70	—
	03:14:31.9	42:46:15.6	0.0303	12.8	7.9	0.123[e]	1.131[e]	1.79	—
	03:14:40.5	39:37:03.2	0.0151[a]	12.8	6.0	0.990[d]	4.820[d]	2.62	UGC02604
	03:15:01.4	42:02:08.5	0.0233[a]	12.5	94.6	8.166	11.110	2.06	UGC02608
	03:16:00.7	40:53:10.0	0.0157[a]	12.7	4.1	0.880[d]	4.510[d]	2.74	UGC02617
	03:16:43.0	41:19:29.3	0.0189[a]	11.9	562.2[b]	0.468	1.992	0.28	IC0310
	03:16:45.9	40:19:47.5	0.0164[a]	13.5	5.5	1.298	3.212	2.60	—
	03:16:46.7	40:00:12.6	0.0142	12.2	36.0	0.126[e]	1.464[e]	1.22	IC0311
	03:17:51.1	41:27:02.8	0.0150	13.0	31.7[h]	0.260[d]	1.206[e]	1.30	—
	03:17:52.4	43:18:13.7	0.0204[a]	12.9	20.9	2.131	4.084	2.19	UGC02640
	03:18:15.7	41:51:27.7	0.0251[a]	11.7	5369.1[b]	0.162[e]	0.747[e]	-1.14	NGC1265
	03:18:43.3	42:17:59.8	0.0193[a]	12.7	12.5	1.760[d]	4.680[d]	2.39	UGC02654
	03:18:45.3	43:14:19.7	0.0207[a]	12.9	5.8	0.810[d]	0.990[d]	2.25	UGC02655
	03:18:58.2	41:28:11.4	0.0162[a]	12.6	12.6[h]	0.117[e]	0.612[e]	1.39	NGC1270
	03:19:21.4	41:29:25.8	0.0134[a]	11.7	12.5[h]	0.126[e]	1.164[e]	1.60	NGC1272
	03:19:34.3	41:34:48.9	0.0147[a]	12.7	12.8[h]	0.144[e]	1.404[e]	1.67	IC1907
	03:19:48.3	41:30:41.3	0.0176[a]	11.4	22820.	7.146	6.981	-0.43	3C84
	03:19:51.6	41:34:23.7	0.0166[a]	12.5	2.7[h]	0.320[d]	1.035[d]	2.36	NGC1277
	03:19:54.2	41:33:47.2	0.0202[a]	12.0	4.7[h]	0.510[d]	0.978[d]	2.21	NGC1278
	03:20:12.2	41:22:00.3	0.0072	12.3	5.4[h]	0.210[d]	0.864[e]	1.94	NGC1282
	03:20:22.0	41:38:25.4	0.0125[a]	13.8	5.1[h]	0.430[d]	0.648[e]	2.06	—
	03:21:40.0	41:21:36.2	0.0222	12.3	4.3[h]	0.460[d]	0.711[e]	2.17	NGC1294
	03:22:03.0	40:51:49.4	0.0214[a]	12.4	3.5	0.093[e]	1.002[e]	2.08	UGC02698
	03:22:05.3	42:10:17.2	0.0182[a]	13.5	3.3	0.150[d]	0.621[e]	2.01	UGC02696
	03:24:23.0	40:47:19.4	0.0130	13.7	57.5	0.470[d]	1.080[e]	1.13	—
	03:24:43.9	41:58:07.9	0.0229[a]	13.4	10.1	1.333	3.262	2.35	UGC02718
	03:25:05.4	40:33:30.3	0.0234[a]	12.7[g]	29.6	7.157	10.420	2.52	—
	03:25:09.4	42:24:05.3	0.0119[a]	13.1	3.8	0.707	3.282	2.65	UGC02722
	03:25:25.8	40:32:10.0	0.0121	12.7[g]	14.3	1.010[d]	4.840[d]	2.24	—
	03:25:52.5	40:44:53.7	0.0126[a]	13.2	19.0	1.780[d]	4.580[d]	2.21	UGC02730
	03:25:59.2	40:47:19.8	0.0233[a]	12.5	5.3	1.040[d]	4.070[d]	2.63	IC0320
	03:26:00.6	42:01:28.4	0.0308	14.5	3.1	0.570[d]	2.180[d]	2.60	UGC02731

Table 5—Continued

Cluster	RA (J2000)	Dec (J2000)	z	m	$S_{1.4GHz}$ [mJy]	$S_{60\mu m}$ [Jy]	$S_{100\mu m}$ [Jy]	q	Common Name
	03:26:34.8	41:41:41.7	0.0142	13.5	3.5	0.190[d]	3.180[d]	2.55	—
	03:27:47.9	40:02:01.5	0.0136[a]	14.1	2.9	0.390[d]	1.278[d]	2.42	UGC02743
	03:27:55.3	39:59:48.7	0.0251	13.5	5.4	0.410[d]	2.280[d]	2.32	—
	03:27:59.3	39:54:14.8	0.0145[a]	13.2	4.4	0.560[d]	1.110[d]	2.29	—
	03:28:27.8	40:09:15.6	0.0142[a]	12.6	43.3	5.309	8.393	2.23	—
	03:30:01.8	41:49:56.0	0.0143[a]	12.6[g]	13.4	4.556	9.668	2.73	NGC1334
A539	05:13:24.0	07:31:35.0	0.0302	14.6	2.7	0.690[d]	1.317[e]	2.59	—
	05:13:30.4	07:25:06.5	0.0289	14.3	5.2	0.288[e]	0.873[e]	2.02	—
	05:13:46.3	05:42:54.2	[i]	13.8[g]	7.9	0.730[d]	0.747[e]	2.05	—
	05:14:07.0	06:31:13.5	0.0298[a]	13.3	5.3	0.710[d]	2.690[d]	2.46	UGC03269
	05:14:53.1	06:15:02.2	0.0288[a]	13.8	3.4	0.560[d]	1.140[d]	2.30	—
	05:15:36.7	07:11:53.7	0.0297[a]	13.8	6.1	0.700[d]	2.200[d]	2.34	—
	05:15:50.6	06:13:39.1	0.0311[a]	14.5	5.1	0.510[d]	0.910[d]	2.17	—
	05:16:05.7	05:34:28.4	0.0278[a]	14.0	4.5	0.180[d]	1.030[d]	2.05	—
	05:16:14.2	06:06:23.7	0.0310[a]	13.9	5.5	0.930[d]	2.370[d]	2.46	UGC03272
	05:16:26.5	06:28:08.4	0.0339[a]	12.8[g]	3.8	0.450[d]	1.250[e]	2.33	—
	05:16:26.6	06:50:48.8	0.0335[a]	14.4	3.7	0.126[e]	0.450[e]	1.85	—
	05:16:46.3	06:37:19.7	0.0266[a]	14.0	4.1	0.123[e]	1.770[e]	2.23	UGC03275
	05:16:55.2	06:33:07.7	0.0323[a]	12.9	24.6	0.132[e]	0.822[e]	1.20	—
	05:17:09.9	06:55:36.8	0.0283	13.6	4.3	0.780[d]	4.164[e]	2.68	UGC03279
	05:19:12.8	05:52:40.4	0.0307	14.4	6.5	0.380[d]	0.840[e]	1.97	—
	05:19:33.7	05:25:43.8	0.0298[a]	14.7	2.9	0.250[d]	1.302[e]	2.35	—
	05:19:51.5	05:29:59.5	0.0292	14.4	2.6	0.201[e]	0.771[e]	2.22	—
	05:20:06.1	06:34:54.7	0.0296[a]	14.1	7.2	0.770[d]	2.700[d]	2.34	UGC03289
	05:20:12.3	05:55:17.9	0.0288[a]	14.2	3.2	0.560[d]	2.480[d]	2.61	—
	05:20:12.6	05:50:11.5	0.0286[a]	13.7	19.7	1.760[d]	2.970[d]	2.11	—
	05:21:45.8	06:41:18.5	0.0300	13.0	4.8	1.190[d]	3.702[e]	2.68	NGC1875
	05:21:49.9	06:40:35.7	0.0317	14.6	7.6	1.200[d]	3.432[e]	2.46	Arp327
A569	07:02:33.1	50:35:26.2	0.0210	12.7	3.6	0.490[d]	1.490[d]	2.41	—
	07:03:03.1	49:25:29.0	0.0189	13.0	5.4	0.519	2.199	2.34	UGC03638
	07:05:42.0	50:34:51.6	0.0197	11.9	19.7	0.246	1.237	1.50	NGC2320
	07:07:51.7	48:24:51.1	0.0184	14.6	8.0	0.162[e]	0.405[e]	1.54	—
	07:08:10.9	50:40:55.1	0.0201	12.2	11.1	0.294	1.582	1.85	NGC2326
	07:08:34.2	50:37:52.2	0.0205	13.6	3.0	0.570[d]	1.240[d]	2.48	NGC2326A
	07:09:08.0	48:36:56.1	0.0197	12.1	753.7[b]	0.135[e]	0.495[e]	-0.42	NGC2329
	07:09:23.0	48:38:07.9	0.0206	12.7	5.8	0.102[e]	0.441[e]	1.61	UGC03696
	07:09:34.2	50:10:56.2	0.0196	12.3	121.4	0.108[e]	0.303[e]	0.21	NGC2332

Table 5—Continued

Cluster	RA (J2000)	Dec (J2000)	z	m	$S_{1.4GHz}$ [mJy]	$S_{60\mu m}$ [Jy]	$S_{100\mu m}$ [Jy]	q	Common Name
	07:10:34.2	50:07:07.8	0.0214	12.8	3.1	0.090[e]	1.490[d]	2.27	IC0458
	07:11:41.6	49:51:44.1	0.0206	12.4	8.5	0.093[e]	0.426[e]	1.42	UGC03725
	07:12:43.7	50:03:42.7	0.0184	13.9	8.3	0.102[e]	0.297[e]	1.36	—
	07:16:52.3	49:52:29.4	0.0210	14.3	2.7	0.560	1.215	2.52	—
	07:22:18.6	49:17:32.1	0.0206	12.5	8.7	0.369	1.457	1.97	UGC03812
A634	08:08:44.7	56:35:31.2	0.0272	13.8	3.2	0.362	0.807	2.26	—
	08:09:39.6	57:31:27.5	0.0255	14.6	2.4	0.105[e]	0.597[e]	2.08	—
	08:09:52.6	57:54:44.8	0.0266	13.2	5.4	0.114[e]	0.300[e]	1.57	—
	08:11:53.6	57:57:05.3	0.0279[a]	14.1	11.2	1.363	2.557	2.26	—
	08:11:57.5	58:42:02.9	0.0283[a]	13.7	3.9	0.264	0.835	2.12	—
	08:12:08.5	57:54:26.7	0.0260[a]	14.6	3.8	0.320[d]	1.580[d]	2.33	—
	08:12:17.2	58:33:50.6	0.0269	14.0	6.2	0.230[d]	0.580[d]	1.80	—
	08:12:50.6	57:55:15.9	0.0267	13.5	4.6	0.450[d]	0.830[d]	2.16	—
	08:14:15.5	58:11:57.7	0.0260[a]	15.0	2.7	0.426	0.711	2.35	—
	08:15:44.9	58:19:14.1	0.0271	12.5	6.7	0.950[d]	2.210[d]	2.37	UGC04289
	08:16:01.5	58:20:00.7	0.0253[a]	14.4	8.2	1.092	2.376	2.33	—
	08:18:10.6	57:45:31.2	0.0247[a]	13.9	4.2	0.438	0.848	2.20	—
	08:22:02.7	57:18:29.4	0.0267	13.8	2.7	0.180[d]	0.456[e]	2.06	—
A779	09:18:35.6	34:33:11.1	0.0212[a]	13.5	5.4	0.444	1.419	2.20	UGC04926
	09:19:17.5	34:00:30.1	0.0238[a]	13.8	228.2	0.078[e]	0.234[e]	-0.19	NGC2823
	09:19:24.2	33:37:26.8	0.0213	13.5	3.4	0.280[d]	0.440[d]	2.06	NGC2826
	09:19:41.4	33:44:18.0	0.0208	13.6	2.8	0.480[d]	1.310[d]	2.49	NGC2830
	09:19:46.6	33:44:57.5	0.0232	12.2	5.5	0.450[d]	1.290[d]	2.18	NGC2832
	09:20:37.0	33:04:29.5	0.0216[a]	14.2	4.7	0.480	1.008	2.21	—
	09:20:52.7	35:22:05.6	0.0250[a]	13.2	5.6	0.594	1.916	2.32	NGC2840
	09:21:51.5	33:24:06.9	0.0236[a]	13.2	113.8	0.171[e]	0.354[e]	0.37	UGC04972
A1185	11:04:37.2	28:13:40.6	0.0291[a]	13.3	6.5	0.613	1.640	2.22	NGC3515
	11:05:53.8	28:48:00.4	0.0331	14.0	2.7	0.230[d]	1.530[d]	2.42	UGC06147
	11:07:08.7	28:35:32.6	0.0338	13.9	8.3	0.300[d]	0.380[d]	1.67	UGC06166
	11:08:30.3	29:50:13.2	0.0355	14.0	4.0	0.450[d]	1.270[d]	2.31	—
	11:09:25.8	29:34:09.3	0.0347[a]	13.7	4.0	0.307	0.860	2.14	UGC06198
	11:09:33.1	28:37:39.9	0.0381	14.5	3.9	0.180[d]	1.940[d]	2.32	—
	11:10:47.8	28:39:37.1	0.0292[a]	13.8	41.3	0.117[e]	0.480[e]	0.80	NGC3554
	11:10:55.3	28:28:10.3	0.0317[a]	14.4	4.6	0.321	0.975	2.12	—
	11:10:55.9	28:32:37.5	0.0321	13.4	4.1	0.120[e]	0.522[e]	1.83	NGC3558
	11:10:59.9	29:20:11.7	0.0293	14.2	7.6	0.320[d]	0.400[d]	1.73	UGC06220
	11:11:13.0	28:42:42.6	0.0289	13.8	24.4	4.180	6.719	2.38	UGC06224

Table 5—Continued

Cluster	RA (J2000)	Dec (J2000)	z	m	$S_{1.4GHz}$ [mJy]	$S_{60\mu m}$ [Jy]	$S_{100\mu m}$ [Jy]	q	Common Name
	11:11:13.2	28:41:47.0	0.0287	13.4	42.6	4.140[d]	7.390[d]	2.15	NGC3561
	11:11:19.2	28:40:51.4	0.0294	14.3	3.1	3.300[d]	6.500[d]	3.21	—
	11:12:04.0	27:34:01.2	0.0366	14.7	3.2	0.160[d]	0.372[e]	1.92	—
	11:13:10.4	27:49:05.7	0.0314	13.3	4.2	0.141[d]	0.740[d]	1.95	UGC06250
	11:13:11.3	28:00:43.5	0.0321	14.8	2.7	0.093[e]	0.680[d]	2.06	—
	11:16:10.7	29:26:31.8	0.0278[a]	14.4	5.0	1.129	1.761	2.50	—
A1267	11:24:10.7	27:00:49.9	0.0330	13.9	3.4	—	—	—	UGC06415
	11:24:24.0	27:42:44.3	0.0324	14.9	27.4	—	—	—	—
	11:28:25.3	27:27:18.8	0.0335	14.8	8.6	—	—	—	—
	11:30:28.0	25:48:57.2	0.0336	14.6	4.5	—	—	—	—
	11:30:53.4	26:19:27.4	0.0332	14.5	6.3	—	—	—	—
	11:31:09.5	26:13:33.5	0.0334	14.2	12.7	—	—	—	—
	11:31:45.8	26:28:30.7	0.0328	14.3	7.5	—	—	—	—
A1367	11:36:20.1	20:31:17.5	0.0218[a]	13.5	6.8	0.153[e]	0.774[e]	1.76	—
	11:36:54.3	19:59:47.9	0.0221[a]	13.4	3.0	2.290[d]	4.720[d]	3.07	—
	11:36:54.3	19:58:15.3	0.0206	13.4	18.9	2.108	4.494	2.25	UGC06583
	11:40:41.7	20:20:33.7	0.0218[a]	12.2	4.3	0.213[e]	1.210[d]	2.14	NGC3085
	11:42:24.6	20:07:07.8	0.0201	13.3	13.4	1.874	3.914	2.34	—
	11:42:56.5	19:57:55.5	0.0245	14.3	22.5	0.270[d]	0.390[e]	1.21	—
	11:43:13.3	20:00:16.0	0.0234	14.5	5.5	0.334	0.637	1.96	—
	11:43:48.6	19:58:11.0	0.0221	13.0	54.8	1.524	2.879	1.62	UGC06697
	11:43:58.2	20:48:21.8	0.0213	14.5	3.2	0.389	1.223	2.37	—
	11:43:58.3	20:11:05.6	0.0213[a]	14.0	3.2	0.440[d]	0.480[e]	2.23	—
	11:43:59.0	20:04:35.9	0.0246[a]	13.3	4.6	0.818	1.454	2.42	NGC3840
	11:44:02.2	19:56:58.1	0.0208[a]	11.9	12.6	0.200[d]	0.603[e]	1.47	NGC3842
	11:44:47.1	20:07:28.9	0.0219[a]	12.8	3.1	0.130[d]	0.660[d]	2.03	UGC06719
	11:44:47.7	19:46:22.4	0.0277[a]	14.6	7.4	1.020	3.190	2.42	—
	11:44:49.4	19:47:41.2	0.0190	12.8	17.9	0.786	2.555	1.94	NGC3860
	11:44:52.4	19:27:14.8	0.0182[a]	13.4	11.1	0.986	2.399	2.18	NGC3859
	11:44:54.9	19:46:34.3	0.0276	13.7	2.5	0.750[d]	2.340[d]	2.76	—
	11:45:04.0	19:58:24.3	0.0171	12.4	11.9	0.437	1.655	1.90	NGC3861
	11:45:05.1	19:36:21.0	0.0214[a]	12.4	5490.[b]	0.171[e]	0.435[e]	-1.27	NGC3862
	11:45:17.7	20:01:09.9	0.0179[a]	13.9	4.8	0.530[d]	1.110[d]	2.24	—
	11:45:27.8	20:48:24.7	0.0231[a]	13.1	9.9	0.120[e]	0.414[e]	1.39	—
	11:45:49.0	20:37:42.0	0.0235	13.8	3.6	0.629	1.176	2.42	—
	11:45:59.9	20:26:18.8	0.0243[a]	13.3	19.4	4.014	6.529	2.47	IC732
	11:46:12.3	20:23:28.6	0.0232	13.4	14.9	0.129[e]	1.340[d]	1.58	NGC3884

Table 5—Continued

Cluster	RA (J2000)	Dec (J2000)	z	m	$S_{1.4GHz}$ [mJy]	$S_{60\mu m}$ [Jy]	$S_{100\mu m}$ [Jy]	q	Common Name
	11:46:46.8	21:16:16.1	0.0223	13.6	3.7	0.429	0.965	2.27	MRK0640
	11:50:52.4	21:10:14.2	0.0259	13.1	3.7	0.532	1.845	2.47	—
	11:50:55.6	21:08:42.0	0.0214[a]	13.8	5.4	0.920[d]	2.260[d]	2.46	MRK1461
	11:51:01.2	20:23:56.2	0.0215[a]	12.4	3.3	0.440[d]	1.380[d]	2.41	UGC6821
	11:52:01.3	20:39:31.4	0.0203	14.2	2.8	0.325	0.843	2.30	—
A1656	12:52:53.7	28:22:14.5	0.0237	13.0	29.7	1.878	5.019	2.05	UGC08017
	12:54:19.1	27:04:03.0	0.0275[a]	12.6	73.2	0.117[e]	0.157[e]	0.32	NGC4789
	12:56:06.2	27:40:39.2	0.0166[a]	14.7	6.6	0.550[d]	1.030[d]	2.10	MRK0053
	12:56:43.6	27:10:41.4	0.0253[a]	13.1	65.7[b]	0.180[d]	0.430[d]	0.76	NGC4827
	12:57:24.4	27:29:50.4	0.0246[a]	12.1	75.3	0.078[e]	0.291[e]	0.34	NGC4839
	12:57:25.4	27:24:15.2	0.0162	14.3	3.0	0.110[d]	0.510[d]	1.95	MRK0055
	12:57:31.3	26:30:42.2	0.0241	14.3	7.4	0.437	1.221	2.03	IC0837
	12:57:57.9	28:03:39.4	0.0273	14.2	5.1	0.130[d]	0.590[d]	1.79	—
	12:58:05.6	28:14:32.6	0.0245	13.1	23.3	1.342	2.600	1.94	NGC4848
	12:58:09.4	28:42:29.5	0.0254[a]	13.8	6.3	0.310	0.969	1.97	—
	12:58:12.8	26:23:46.9	0.0195[a]	13.1	50.0	0.250[d]	0.580[d]	0.92	NGC4849
	12:58:35.3	27:35:45.1	0.0258	13.3	3.1	0.653	1.477	2.53	NGC4853
	12:58:35.4	27:15:51.1	0.0246[a]	14.5	4.5	0.162[e]	1.060[d]	2.05	MRK0056
	12:58:37.3	27:10:33.3	0.0257	14.8	6.0	0.359	0.761	1.98	MRK0057
	12:59:02.2	28:06:54.5	0.0315[a]	14.2	7.7	0.415	0.972	1.95	NGC4858
	12:59:05.3	27:38:37.5	0.0185[a]	13.8	3.8	0.378	0.578	2.14	MRK0058
	12:59:23.4	27:54:40.8	0.0226[a]	13.1	445.6[c]	0.114[e]	0.438[e]	-0.01	NGC4869
	12:59:35.7	27:57:32.3	0.0239[a]	11.9	214.1[b]	0.141[e]	0.309[e]	0.02	NGC4874
	13:00:33.8	27:38:13.8	0.0251	14.3	4.8	0.165[e]	0.410[d]	1.77	—
	13:00:35.8	27:34:25.4	0.0170[a]	14.3	2.6	0.240[d]	1.450[d]	2.43	—
	13:00:38.0	28:03:24.7	0.0258	14.1	23.2	1.225	2.557	1.92	IC4040
	13:00:40.7	28:31:08.6	0.0297	14.5	8.1	0.129[e]	0.273[e]	1.40	—
	13:00:56.1	27:47:25.0	0.0270	12.3	20.3	0.777	2.462	1.87	NGC4911
	13:01:24.8	29:18:48.0	0.0235	12.3	39.3	6.510[d]	7.400[d]	2.32	NGC4922[j]
	13:01:25.2	28:40:36.4	0.0292[a]	13.6	4.3	0.336	1.004	2.16	—
	13:01:33.7	29:07:48.6	0.0246	13.0	6.1	0.135[e]	0.300[d]	1.55	IC8043
	13:01:43.5	29:02:39.2	0.0237[a]	13.1	2.8	0.436	1.214	2.45	IC4088
	13:01:57.7	28:00:19.6	0.0260	12.9	6.4	0.130[d]	0.520[d]	1.65	NGC4927
	13:02:08.0	27:38:52.5	0.0240[a]	13.8	2.5	0.558	0.942	2.51	NGC4926A
	13:02:12.9	28:12:51.9	0.0273[a]	14.3	2.8	0.350[d]	0.740[d]	2.29	—
	13:03:29.2	26:33:00.0	0.0223[a]	13.8	3.9	0.229	0.747	2.06	UGC08161
	13:04:18.5	28:28:03.6	0.0259[a]	14.2	20.7	0.117[e]	0.492[e]	1.11	—

Table 5—Continued

Cluster	RA (J2000)	Dec (J2000)	z	m	$S_{1.4GHz}$ [mJy]	$S_{60\mu m}$ [Jy]	$S_{100\mu m}$ [Jy]	q	Common Name
	13:04:22.8	28:48:37.6	0.0268^{a}	14.1	3.3	0.228	0.494	2.04	—
	13:06:17.3	29:03:46.4	0.0236	12.6	18.4	0.718	2.232	1.87	NGC4966
	13:06:36.5	27:52:21.1	0.0210	14.0	7.8	0.904	2.083	2.28	—
A2162	16:09:43.1	30:27:09.0	0.0309	13.5	3.0	0.080^{d}	0.510^{d}	1.90	UGC10234
	16:12:34.1	28:19:07.1	0.0315^{a}	14.2	4.4	0.860^{d}	3.670^{d}	2.65	—
	16:12:35.6	29:29:04.1	0.0313^{a}	12.8	113.4^{c}	0.126^{e}	0.552^{e}	0.41	NGC6086
	16:12:38.9	29:38:36.0	0.0321^{a}	13.7	27.7	0.102^{e}	0.462^{e}	0.94	—
A2197	16:21:22.2	40:48:36.4	0.0303	14.7	5.5	0.280^{d}	0.820^{d}	1.97	UGC10354
	16:21:41.7	40:35:27.2	0.0312	14.7	3.4	0.536	1.286	2.42	—
	16:22:00.2	40:26:51.3	0.0309^{a}	14.3	3.2	0.296	0.916	2.25	UGC10357
	16:23:23.0	41:39:02.9	0.0275^{a}	13.8	7.0	1.100	2.294	2.39	—
	16:28:28.2	41:13:04.4	0.0282^{a}	13.6	19.8	1.622	3.120	2.09	UGC10407
	16:29:00.4	41:17:01.8	0.0318^{a}	13.4	3.5	0.454	1.325	2.38	UGC10415
A2199	16:20:55.9	39:51:38.6	0.0288	15.2	8.7	0.930^{d}	2.580^{d}	2.28	—
	16:21:05.1	39:55:01.1	0.0322^{a}	13.9	2.4	0.410^{d}	2.050^{d}	2.64	—
A2197/99	16:22:53.9	40:29:45.8	0.0310	14.8	11.1	0.786	1.182	1.99	MRK0880
A2197/99	16:23:16.6	39:55:10.4	0.0322	12.9	6.7	0.387	1.303	2.06	UGC10367
	16:24:17.8	39:12:39.8	0.0300	13.9	4.3	0.093^{e}	0.183^{e}	1.52	—
	16:24:37.2	39:07:38.5	0.0349	14.3	8.5	1.743	3.711	2.51	—
	16:25:04.8	39:45:29.2	^{i}	14.5	38.0^{c}	0.641	1.608	1.46	—
A2197/99	16:25:10.4	40:53:33.2	0.0290^{a}	12.7	176.5^{b}	0.120^{d}	0.441^{e}	0.19	NGC6146
	16:25:23.7	38:48:22.4	0.0315	14.6	3.6	0.389	1.086	2.29	—
A2197/99	16:25:31.5	40:08:12.9	0.0328	14.9	7.6	0.536	1.369	2.09	—
A2197/99	16:25:44.5	40:28:31.3	0.0317	14.2	5.3	0.562	1.567	2.28	—
A2197/99	16:25:49.3	40:20:41.5	0.0290^{a}	14.1	15.0	1.395	2.629	2.14	MRK0881
A2197/99	16:25:50.0	40:29:18.3	0.0290	13.1	32.4	0.560^{d}	1.520^{d}	1.49	NGC6150
A2197/99	16:26:14.3	39:58:00.7	0.0325^{a}	13.8	5.9	0.777	2.171	2.38	—
	16:26:37.1	39:07:37.8	0.0353^{a}	14.4	4.1	0.932	1.562	2.51	UGC10389
A2197/99	16:27:11.3	40:54:23.2	0.0318	14.8	5.0	0.361	0.668	1.99	—
	16:27:22.2	39:06:34.0	0.0331^{a}	13.4	7.5	0.550	1.643	2.14	MRK0882
A2197/99	16:28:38.5	39:33:04.4	0.0304^{a}	12.4	3603.^{b}	0.140^{d}	0.500^{d}	-1.10	NGC6166
A2197/99	16:28:39.6	40:07:23.8	0.0260	13.6	8.3^{k}	0.096^{e}	0.324^{e}	1.36	—
A2197/99	16:28:42.3	40:07:25.0	0.0337	13.9	8.3^{k}	0.096^{e}	0.324^{e}	1.36	—
	16:28:58.1	39:19:08.0	0.0346^{a}	14.2	6.2	0.822	1.775	2.32	—
A2197/99	16:29:20.1	39:25:43.1	0.0277	13.7	11.7	0.081^{e}	0.228^{e}	1.10	—
A2197/99	16:29:44.9	40:48:40.6	0.0294^{a}	12.6	8.0	0.108^{e}	0.147^{e}	1.25	NGC6173
A2197/99	16:29:51.1	39:45:58.2	0.0317	13.6	4.3	0.110^{d}	0.320^{d}	1.67	UGC10420

Table 5—Continued

Cluster	RA (J2000)	Dec (J2000)	z	m	$S_{1.4GHz}$ [mJy]	$S_{60\mu m}$ [Jy]	$S_{100\mu m}$ [Jy]	q	Common Name
A2197/99	16:29:57.9	40:37:45.2	0.0293[a]	12.8	12.2	0.120[d]	0.570[d]	1.38	NGC6175
	16:30:32.8	39:23:02.0	0.0305	14.4	18.2	0.679	0.537	1.63	—
A2197/99	16:30:33.4	39:49:49.1	0.0248[a]	13.9	2.7	0.240[d]	0.530[d]	2.16	UGC10429
A2197/99	16:31:34.6	40:33:54.9	0.0277[a]	13.5	4.4	0.526	1.829	2.39	NGC6184
	16:33:49.8	39:15:46.5	0.0318	13.5	11.1	0.668	1.753	2.02	IC4610
A2197/99	16:34:52.5	40:11:39.8	0.0306	14.2	4.3	0.506	1.707	2.37	—
A2634	23:35:50.0	26:59:43.1	0.0237[a]	13.9	7.2	1.461	2.237	2.45	—
	23:36:25.7	27:56:07.3	0.0296	15.0	5.2	0.530[d]	0.990[d]	2.18	UGC12701
	23:38:16.7	26:52:03.8	0.0260[a]	15.5	3.6	0.138[e]	1.080[d]	2.13	—
	23:38:29.5	27:01:55.1	0.0291[a]	12.6	7657.[c]	0.156[e]	0.780[d]	-1.28	3C465
	23:38:38.9	27:00:40.4	0.0312	13.4	<7657.	0.126[e]	0.660[e]	-1.36	IC5342
	23:40:00.9	27:08:00.3	0.0315[a]	12.7	467.8[b]	0.260[d]	1.700[d]	0.23	—
	23:40:22.2	27:11:04.0	0.0335[a]	14.0	62.5[c]	0.111[e]	0.897[e]	0.80	—
	23:40:42.6	27:10:39.5	0.0339[a]	14.6	13.3	2.174	3.898	2.38	—
	23:40:46.9	26:50:07.0	0.0392	13.2	9.7	0.138[e]	1.188[e]	1.73	UGC12733
	23:42:16.6	28:10:51.8	[i]	14.6	11.2	0.260[d]	1.065[e]	1.72	—
	23:42:23.1	27:19:53.2	0.0247[a]	14.3	7.3	0.874	1.928	2.28	—
	23:42:38.5	27:05:28.4	0.0251	13.9	3.6	0.590[d]	0.784[e]	2.33	—
	23:42:46.8	27:17:50.3	0.0248[a]	13.8	12.0	1.169	3.355	2.25	UGC12746
	23:42:50.1	27:32:58.2	0.0237	15.5	23.6	1.040[d]	0.770[e]	1.69	—
A2634/2666	23:44:01.2	27:42:53.9	0.0248	13.7	3.1	0.420[d]	0.580[e]	2.26	MRK1133
A2666	23:45:07.0	28:12:19.1	0.0241	13.8	3.9	0.140[d]	1.130[d]	2.11	—
	23:45:32.4	27:21:37.7	0.0260	13.1	4.5	0.510[d]	1.870[d]	2.38	NGC7747
	23:45:47.5	27:20:19.9	0.0307	13.9	3.4	0.640[d]	1.910[d]	2.55	—
	23:47:24.6	28:23:35.7	0.0301[a]	13.9	7.8	0.800[d]	2.560[d]	2.30	—
	23:47:34.4	28:26:06.1	0.0301	14.9	9.2	1.192	3.044	2.35	—
	23:47:43.3	27:25:36.9	0.0310[a]	14.1	7.2	0.679	1.426	2.17	—
	23:49:55.3	28:40:04.2	0.0311[a]	14.3	6.7	0.686	1.954	2.27	—
	23:50:47.5	27:17:15.7	0.0267[a]	13.7	3.3	0.445	0.898	2.32	—
	23:52:24.7	28:46:22.1	0.0225[a]	13.2	16.9	1.854	4.027	2.24	NGC7775
	23:55:08.0	27:59:07.8	0.0303	14.9	4.2	0.114[e]	0.620[d]	1.86	—
	23:55:50.5	26:50:54.3	0.0266	14.3	3.0	0.630[d]	0.490[d]	2.37	—
	23:57:26.0	26:50:18.2	0.0256[a]	15.1	6.1	0.554	1.219	2.16	—

Table 5—Continued

Cluster	RA (J2000)	Dec (J2000)	z	m	$S_{1.4GHz}$ [mJy]	$S_{60\mu m}$ [Jy]	$S_{100\mu m}$ [Jy]	q	Common Name

[a] Redshift found in NED.

[b] Resolved radio source. The flux was determined directly from the NVSS image.

[c] Extended radio source (see Table 2).

[d] IRAS detection, with data from *xscanpi* (see text).

[e] Non-detection. The value quoted is a 3σ upper limit based on the local rms reported by *xscanpi*.

[f] This is actually a pair of elliptical galaxies. The redshift presented is the average of the NED values for the two individual galaxies, 0.0238 and 0.0222. Note also that the position and magnitude listed in this table are for the galaxy pair taken together.

[g] Magnitude contaminated by star.

[h] Source accepted from Sijbring list. Flux is the 21 cm Sijbring value modified to 20 cm assuming a spectral index of 0.8.

[i] No redshift was obtained for these objects.

[j] Part of galaxy pair or system. This galaxy is most likely to be the radio source on account of either its optical spectrum or magnitude.

[k] This is a pair of galaxies. The NVSS peak and integral flux likely represents contributions from each individual galaxy. The pair is depicted in Figure 1.

Note. — Column legend — (1) ACO cluster designation; (2) Right Ascension of radio galaxy, based on the optical position in J2000 coordinates; (3) Declination of radio galaxy, based on the optical position in J2000 coordinates; (4) Heliocentric redshift of the galaxy, where a flag indicates the redshift was found in NED; (5) Apparent Gunn-Oke magnitude of the galaxy, derived from the POSS II (see text); (6) 1.4GHz radio flux of the galaxy, taken from the NVSS. For sources contained within larger extended radio emission (see Table 2), the flux is an upper limit and denoted with a less than sign; (7) & (8) IRAS 60 μm flux and 100 μm flux, if available. Unless noted otherwise, the flux is taken from either the IRAS Faint Source Catalog or Point Source Catalog; (9) q value for the galaxy, derived from columns (6) – (8). Note that the reported q value may represent an upper limit (see flags for columns (7) & (8)); (10) Name of galaxy in other common catalogs, with preference given to the NGC and UGC catalogs.

Table 6. Non-Cluster Radio Galaxy Data

Cluster	RA (J2000)	Dec (J2000)	z	m	$S_{1.4GHz}$ [mJy]	$S_{60\mu m}$ [Jy]	$S_{100\mu m}$ [Jy]	q	Common Name
A262	01:58:04.5	34:17:58.8	0.0476[a]	13.4	34.6	0.105[e]	0.730[d]	0.99	—
	01:47:35.8	37:37:23.3	0.0744	14.0	8.5	0.160[d]	0.570[d]	1.59	—
	01:50:40.4	37:23:07.6	0.0737	13.8	128.0	0.126[e]	0.234[e]	0.17	—
	01:54:17.1	34:18:54.6	0.0859	13.6	23.3	0.210[d]	0.530[d]	1.19	—
	01:59:58.3	37:23:31.2	0.0489	14.0	7.6	0.084[e]	0.225[e]	1.29	—
A347	02:13:58.8	41:20:29.5	0.0874	14.2	2.9	0.170[d]	0.910[d]	2.19	—
	02:16:12.0	42:49:19.1	0.0457[a]	13.1	3.2	0.480[d]	1.300[d]	2.43	UGC01743
	02:24:29.5	40:52:12.5	0.0434	13.0	3.3	0.730[d]	1.640[d]	2.55	UGC01855
	02:26:13.0	39:45:49.8	0.0755	13.7	4.7	0.220[d]	0.255[e]	1.77	—
	02:28:14.9	42:11:44.8		14.4	296.3[f]	0.087[e]	0.350[e]	-0.19	—
	02:33:24.0	42:52:31.3	0.0432	14.1	5.8	0.560	1.443	2.22	—
	02:33:29.1	40:13:36.7	0.0560	14.0	3.4	0.294[e]	0.543[e]	2.11	—
	02:33:43.6	40:05:44.7	0.0360	12.9	4.1	0.490[d]	0.900[d]	2.25	—
	02:34:53.4	41:07:05.9	0.0630	13.3	2.7	0.180[d]	0.450[d]	2.06	UGC02058
A397	02:54:05.4	14:54:08.8	0.1063	15.5	3.9	0.120[e]	0.474[e]	1.83	—
	02:54:10.7	15:43:46.0	0.0758	15.2	7.4	0.120[d]	0.309[e]	1.45	—
	02:54:29.6	14:50:49.7	0.1065	15.5	21.3	0.108[e]	0.279[e]	0.94	—
	02:57:16.0	15:43:02.3	0.0779	15.3	3.6	0.130[d]	0.710[d]	1.99	—
	02:59:19.1	16:04:38.0	0.0683	15.7	2.6	0.280[d]	0.960[e]	2.34	—
	02:59:59.8	15:09:34.0	0.0724	15.3	3.5	0.330[d]	1.692[d]	2.39	—
	03:02:11.2	15:55:38.0	0.0170	14.6	2.9	1.116	1.378	2.69	—
A400	02:52:46.0	06:39:19.4	0.0627	14.7	5.2	0.123[e]	0.786[e]	1.85	—
	02:56:25.8	06:56:23.3	0.1167	14.7	548.8	0.243[e]	1.836[e]	0.18	—
	02:57:57.1	05:17:00.1	0.0165	14.8	3.6	0.393	<1.477	2.37	—
	02:58:51.2	06:22:24.6	0.0451[a]	14.0	7.7	0.620[d]	2.770[d]	2.28	—
	02:59:35.6	06:05:46.3	0.0342	15.0	4.4	0.373	<1.996	2.35	—
A426	03:06:55.6	41:37:24.5	0.0494	13.3[g]	3.1	0.132[e]	1.176[d]	2.22	—
	03:08:12.8	42:26:31.5	0.0655	13.4[g]	10.0	0.144[e]	0.744[e]	1.57	—
	03:11:55.8	41:41:38.3	0.0316	14.3	4.8	0.310[d]	1.200[d]	2.15	—
	03:20:31.3	43:06:50.9	0.0524	13.2	484.7	0.147[e]	0.837[e]	-0.07	—
	03:20:38.2	43:04:44.1	0.0517	13.1	781.8	0.072[e]	0.330[d]	-0.65	—
	03:23:26.2	39:06:35.1	0.0411	14.1	3.0	0.114[e]	1.410[e]	2.28	—
	03:25:03.4	40:58:29.4	0.0466	14.3[g]	2.6	0.171[e]	0.924[e]	2.25	—
	03:26:00.6	42:01:28.4	0.0308	14.5	3.1	0.570[d]	2.180[d]	2.60	UGC02731
	03:28:21.2	43:10:40.6	0.0318	12.6[g]	51.8	0.228[e]	1.350[e]	1.10	—
A539	05:11:20.3	06:21:50.6	0.1042	15.1	4.9	0.105[e]	0.312[e]	1.60	—
	05:12:08.8	05:27:42.3	0.0147[a]	13.7	3.9	1.140[d]	2.240[d]	2.65	—

Table 6—Continued

Cluster	RA (J2000)	Dec (J2000)	z	m	$S_{1.4GHz}$ [mJy]	$S_{60\mu m}$ [Jy]	$S_{100\mu m}$ [Jy]	q	Common Name
	05:12:45.4	06:16:03.9	0.0406^{a}	14.5	3.6	3.070^{d}	3.360^{d}	3.02	—
	05:12:46.6	06:17:46.7	0.0429^{a}	14.7	13.3	2.993	3.902	2.47	—
	05:15:15.6	06:15:52.1	0.0150^{a}	13.1	11.0	1.180^{d}	2.140^{d}	2.20	—
	05:16:58.4	06:09:58.5	0.0415^{a}	14.1	2.8	0.440^{d}	0.760^{d}	2.36	—
	05:18:31.3	04:57:48.4	0.0694	14.9	6.7	0.473	<1.561	2.14	—
A569	06:58:35.5	47:38:51.9	0.0912	14.1	114.4^{b}	0.111^{e}	0.294^{e}	0.23	—
	06:59:04.3	49:02:35.3	0.0919	14.4	182.9^{b}	0.153^{e}	0.486^{e}	0.21	—
	07:01:52.7	47:39:57.5	0.0536	13.3	12.0	0.280^{d}	1.110^{e}	1.71	—
	07:01:57.6	46:48:40.8	0.0263	14.1	6.3	0.715	1.212	2.21	—
	07:02:06.0	48:59:18.4	0.0649	13.7	38.7	0.140^{d}	0.363^{e}	0.80	—
	07:02:09.1	47:10:48.5	0.0587	13.3	13.2	0.126^{e}	0.486^{e}	1.31	—
	07:07:19.1	48:21:04.7	0.0419	14.5	5.0	0.310^{d}	0.930^{d}	2.07	—
	07:08:51.0	48:41:20.4	0.0632^{a}	14.5	2.3	0.269	<1.038	2.40	—
	07:09:15.9	49:49:13.6	0.0156	13.8	18.3	3.614	4.874	2.42	—
	07:09:17.8	49:52:16.5	0.0165	14.4	4.8	0.226	<2.220	2.29	—
	07:09:37.8	47:26:06.1	0.0607	13.7	5.6	0.153^{e}	0.471^{e}	1.72	—
	07:11:53.2	50:12:38.4	0.0606	14.6	9.8	0.120^{e}	0.294^{e}	1.32	—
	07:12:28.6	47:10:00.7	0.0325^{a}	11.7	2.9	0.499	1.696	2.54	NGC2344
	07:15:43.0	49:35:53.5	0.0333^{a}	14.5	3.0	0.301	<0.944	2.28	—
	07:20:33.5	49:05:17.6	0.0281	13.8	4.3	0.441	1.083	2.24	—
A634	08:09:31.6	58:44:22.6	0.0689	14.3	16.7	0.147^{e}	0.342^{e}	1.16	—
	08:09:40.4	57:53:02.5	0.0890	14.9	2.8	0.084^{e}	0.387^{e}	1.86	—
	08:09:41.1	58:45:12.3	0.0697	13.8	42.8	0.117^{e}	0.276^{e}	0.66	—
	08:13:21.1	57:51:06.4	0.0083^{a}	12.9	3.0	0.250^{d}	0.693^{e}	2.18	UGC04270
	08:20:08.8	56:43:34.3	0.0807	15.1	4.3	0.825	1.217	2.42	—
A779	09:16:46.6	34:25:53.6	0.0563^{a}	13.0	5.3	0.764	1.821	2.38	NGC2793
	09:18:57.9	31:51:10.7	0.0620^{a}	14.8	158.7	0.126^{e}	0.282^{e}	0.11	—
	09:19:27.4	33:47:26.9	0.0194^{a}	14.6	4.9	1.151	2.064	2.54	—
	09:19:29.5	34:18:10.5	0.0460^{a}	14.7	7.1	0.643	1.232	2.14	—
	09:19:54.4	32:56:00.7	0.0499^{a}	13.9	22.2	2.627	4.144	2.22	UGC04947
	09:24:55.1	33:44:12.1	0.0423^{a}	14.3	3.6	0.345	1.018	2.25	—
	09:26:08.2	34:53:43.1	0.0160^{a}	14.7	6.9	0.992	1.487	2.29	MRK0399
A1185	11:04:58.3	29:08:17.0	0.0215^{a}	14.4	2.4	0.224	<0.681	2.25	MRK0036
	11:07:47.0	28:10:34.8	0.0650	15.0	3.2	0.293	<1.094	2.29	—
	11:10:39.0	27:13:52.6	0.0446	14.7	4.0	0.503	0.587	2.20	—
	11:11:48.7	29:40:21.3	0.0563	14.5	3.1	0.220^{d}	0.480^{d}	2.06	—
	11:12:01.8	27:50:54.0	0.0473	14.6	6.7	0.150^{d}	0.723^{e}	1.75	—

Table 6—Continued

Cluster	RA (J2000)	Dec (J2000)	z	m	$S_{1.4GHz}$ [mJy]	$S_{60\mu m}$ [Jy]	$S_{100\mu m}$ [Jy]	q	Common Name
	11:12:32.8	28:01:51.1	0.0475[a]	14.2	3.1	0.130[d]	0.890[d]	2.12	UGC06244
	11:12:34.9	28:02:28.8	0.0459[a]	14.8	2.8	0.110[d]	1.000[d]	2.19	UGC06244
	11:12:54.3	28:00:03.0	0.0467[a]	14.4	3.1	0.305	0.788	2.23	—
	11:15:34.6	29:15:15.4	0.0478[a]	13.7	1929.5	0.186[e]	0.342[e]	-0.84	—
	11:16:22.7	29:15:08.0	0.0453[a]	13.6	73.6	0.129[e]	0.950[d]	0.77	—
	11:16:28.4	29:17:09.3	0.0474[a]	14.2	37.9	0.111[e]	0.324[e]	0.73	—
	11:16:33.3	29:18:44.5	0.0463[a]	14.7	6.3	0.690[d]	2.380[d]	2.35	—
	11:16:33.8	28:46:06.9	0.0234[a]	14.6	3.1	0.450[d]	0.590[d]	2.28	—
A1267	11:23:30.1	27:06:08.5	0.0687	14.5	3.7	—	—	—	—
	11:25:55.4	26:41:20.3	0.0878	14.8	7.9	—	—	—	—
	11:26:15.8	27:51:59.9	0.0241[a]	14.0	9.2	—	—	—	NGC3678
	11:28:11.1	25:39:39.0	0.0091[a]	12.3	28.2	—	—	—	NGC3689
	11:28:15.3	26:14:01.7	0.1068	14.9	4.0	—	—	—	—
	11:28:18.7	26:45:35.0	0.0529[a]	13.9	32.6	—	—	—	—
	11:28:57.2	27:47:45.8	0.0682	14.8	2.7	—	—	—	—
	11:29:12.2	27:33:12.5	0.0732	15.2	67.5	—	—	—	—
	11:30:13.5	26:23:43.5	0.0574	14.6	10.9	—	—	—	—
	11:34:02.3	26:32:22.9	0.0771	14.5	16.5	—	—	—	—
A1367	11:39:47.6	19:56:00.2	0.0366[a]	13.1	18.5	1.110[d]	2.850[d]	2.02	UGC06625
	11:40:05.7	18:13:22.5	0.1242	14.3	3.7	0.117[e]	0.312[e]	1.75	—
	11:41:58.9	18:43:52.7	0.0705	14.1	16.6	0.081[e]	0.327[e]	1.04	—
	11:42:29.0	18:20:08.6	0.0031[a]	12.8	23.2	0.688	1.609	1.69	UGC06670
	11:43:02.2	19:38:57.5	0.0438[a]	13.5	7.0	0.084[e]	0.930[d]	1.74	UGC06680
	11:42:36.3	18:50:42.8	0.0104[a]	12.6	14.3	1.514	3.519	2.24	NGC3827
A1656	12:54:40.6	28:56:18.8	0.0083[a]	11.6	114.7	11.570	26.740	2.22	NGC4793
	12:56:35.3	28:16:28.3	0.0232[a]	14.4	201.5[c]	0.150[e]	0.223[e]	0.01	—
	12:58:18.3	29:07:39.0	0.0266	13.4	8.6[c]	0.130[d]	0.890[d]	1.81	—
	12:59:40.0	27:51:15.6	0.0123[a]	14.5	3.3	0.150[d]	0.760[d]	2.07	—
	13:03:16.7	27:19:55.7	0.0358	14.5	5.2	0.609	1.227	2.26	—
	13:05:47.7	27:44:01.5	0.0085[a]	12.5	9.8	1.048	2.876	2.28	NGC4961
A2162	16:06:31.9	29:27:56.1	0.0917	15.4	3.0	0.428	1.077	2.39	—
	16:06:40.2	30:05:56.0	0.0220[a]	12.7	3.4	0.394	1.538	2.40	UGC10205
	16:08:21.2	28:28:41.6	0.0503[a]	13.8	225.8[b]	0.099[e]	0.540[d]	0.12	IC4590
	16:10:26.8	30:29:15.7	0.1246	15.2	2.9	0.105[e]	0.240[e]	1.77	—
	16:10:52.1	30:02:02.7	0.0994	15.5	2.8	0.300[d]	0.650[d]	2.23	—
	16:11:45.0	29:44:51.6	0.0509	14.2	13.1	0.108[e]	0.288[e]	1.16	UGC10259
	16:12:17.7	28:25:45.2	0.0532	13.8	77.2	0.105[e]	0.489[e]	0.52	—

Table 6—Continued

Cluster	RA (J2000)	Dec (J2000)	z	m	$S_{1.4GHz}$ [mJy]	$S_{60\mu m}$ [Jy]	$S_{100\mu m}$ [Jy]	q	Common Name
	16:12:42.8	29:54:03.0	0.0533	13.8	40.6	0.126[e]	0.550[d]	0.86	—
	16:12:44.9	28:17:06.3	0.0246[a]	13.9	23.0	1.775	4.364	2.12	UGC10273
	16:12:57.0	30:46:14.1	0.0498	14.0	5.3	0.096[e]	0.516[e]	1.69	—
	16:13:04.9	30:54:05.7	0.0508	13.4	7.2	0.150[e]	0.492[e]	1.61	—
	16:13:18.9	30:54:36.4	0.1529	15.4	6.9	0.600[d]	0.453[e]	1.99	—
	16:13:30.2	29:08:35.2	0.0785	14.5	3.8	0.380[d]	2.320[d]	2.47	—
	16:14:28.5	28:17:30.0	0.1069	15.1	424.8	0.093[e]	0.237[e]	-0.42	—
	16:18:29.1	29:58:59.1	0.1340	15.0	144.2[c]	0.078[e]	0.342[e]	0.10	—
A2197	16:28:08.1	42:16:58.6	0.0455	14.2	4.3	0.140[d]	0.276[e]	1.70	—
A2199	16:21:52.3	38:55:57.7	0.0166[a]	13.2	7.8	0.717	2.420	2.26	NGC6131
	16:24:46.1	39:10:50.3	0.1015	15.0	2.9	0.078[e]	0.261[e]	1.72	—
	16:31:07.0	39:25:47.0	0.0636	15.0	3.3	0.249	0.621	2.11	—
A2634	23:35:48.9	26:13:23.5	0.1636	15.4	3.1	0.129[e]	0.471[e]	1.94	—
	23:34:53.9	27:21:06.7	0.0614[a]	14.6	2.4	0.150[d]	0.399[e]	2.04	—
	23:35:01.6	27:22:19.5	0.0613[a]	13.5	78.3	0.099[e]	0.417[e]	0.46	—
	23:36:14.5	26:59:23.2	0.1217[a]	15.1	3.2	0.093[e]	0.384[e]	1.82	—
	23:38:37.7	26:05:44.2	0.0627[a]	15.1	8.0	0.090[e]	0.705[e]	1.60	—
	23:38:58.2	26:03:40.9	0.0612[a]	14.4	4.9	0.105[e]	0.693[e]	1.82	—
	23:39:14.8	27:33:49.4	0.0660	15.3	4.4	0.260[d]	1.227[d]	2.16	—
	23:39:19.0	26:05:31.0	0.0423[a]	15.0	2.6	0.532	1.059	2.50	—
	23:40:15.0	26:58:37.9	0.1772	15.4	11.5	0.141[e]	1.880[d]	1.82	—
	23:41:59.7	26:48:29.5	0.0948[a]	14.1	100.9	0.189[e]	0.858[e]	0.65	3C465H
A2666	23:44:37.1	27:48:33.1	0.0573	13.2	159.2	0.087[e]	0.740[d]	0.31	—
	23:46:52.5	26:56:14.6	0.0731	14.9	4.8	0.520[d]	0.495[e]	2.11	—
	23:48:28.3	27:02:48.6	0.0661	14.2	2.9	0.230[d]	1.290[d]	2.34	—
	23:49:01.6	26:47:17.2	0.0385[a]	13.4	3.3	0.478	1.017	2.36	UGC12792
	23:52:56.7	27:23:04.5	0.0517	15.0	3.1	0.210	<0.736	2.14	—

Table 6—Continued

Cluster	RA (J2000)	Dec (J2000)	z	m	$S_{1.4GHz}$ [mJy]	$S_{60\mu m}$ [Jy]	$S_{100\mu m}$ [Jy]	q	Common Name

[a] Redshift found in NED.

[b] Resolved radio source. The flux was determined directly from the NVSS image.

[c] Extended radio source (see Table 2).

[d] IRAS detection, with data from *xscanpi* (see text).

[e] Non-detection. The value quoted is a 3σ upper limit based on the local rms reported by *xscanpi*.

[f] Overlay shows radio emission originates from background galaxy and not the cluster member.

[g] Magnitude contaminated by star.

Note. — Column legend — (1) ACO cluster designation; (2) Right Ascension of radio galaxy, based on the optical position in J2000 coordinates; (3) Declination of radio galaxy, based on the optical position in J2000 coordinates; (4) Heliocentric redshift of the galaxy, where a flag indicates the redshift was found in NED; (5) Apparent Gunn-Oke magnitude of the galaxy, derived from the POSS II (see text); (6) 1.4GHz radio flux of the galaxy, taken from the NVSS. For sources contained within larger extended radio emission (see Table 2), the flux is an upper limit and denoted with a less than sign; (7) & (8) IRAS 60 μm flux and 100 μm flux, if available. Unless noted otherwise, the flux is taken from either the IRAS Faint Source Catalog or Point Source Catalog; (9) q value for the galaxy, derived from columns (6) – (8). Note that the reported q value may represent an upper limit (see flags for columns (7) & (8)); (10) Name of galaxy in other common catalogs, with preference given to the NGC and UGC catalogs.

Table 7. Absolute Quantities

Cluster	RA (J2000)	Dec (J2000)	M_R	$P_{1.4GHz}$ log[W Hz^{-1}]	L_{FIR} log[L$_\odot$]
A262	01:41:15.6	34:48:40.3	-21.2	21.5	9.8
	01:44:35.5	37:41:46.1	-21.5	22.0	10.2
	01:44:38.3	34:39:35.5	-20.3	21.3	9.5
	01:46:22.7	36:27:35.7	-21.9	21.2	9.8
	01:46:57.0	34:46:19.3	-21.0	21.3	9.6
	01:50:41.1	33:44:25.8	-20.1	21.3	9.6
	01:50:44.3	35:17:03.2	-22.1	21.7	10.0
	01:51:29.3	36:03:56.5	-21.3	22.0	9.9
	01:52:39.7	36:10:15.7	-21.6	21.6	9.4
	01:52:45.9	36:37:06.2	-22.2	21.8	10.1
	01:52:46.5	36:09:07.1	-22.5	22.5	9.6
	01:52:54.1	36:03:11.0	-21.6	22.3	10.1
	01:54:54.0	36:55:03.5	-21.0	22.0	10.6
	01:56:27.8	36:48:07.3	-21.3	21.6	<9.4[a]
	01:56:37.9	34:10:37.9	-21.8	21.3	9.6
	01:56:44.0	36:23:03.6	-21.1	21.2	<8.9[a]
	01:57:42.3	35:54:56.3	-22.5	22.2	10.5
	01:57:50.5	36:20:34.1	-22.2	21.9	9.8
	01:58:54.9	36:40:28.6	-21.7	21.3	9.8
	01:59:05.0	36:15:29.3	-21.5	21.3	9.7
	02:00:55.2	38:12:38.3	-22.2	21.6	10.1
A347	02:13:59.9	41:52:36.5	-21.0	22.0	10.4
	02:18:54.2	42:34:39.0	-20.0	21.9	10.1
	02:19:13.8	41:42:58.4	-21.2	21.7	9.8
	02:20:04.0	41:16:28.2	-21.2	21.7	9.9
	02:21:23.6	42:52:32.6	-21.5	22.1	10.4
	02:22:58.6	43:00:41.7	-22.2	<24.7	<9.2[b]
	02:23:08.1	41:22:10.8	-21.8	<22.1	9.9
	02:23:11.4	41:22:04.5	-21.8	<22.1	9.9
	02:23:11.8	42:59:29.2	-22.9	24.7	9.5
	02:24:44.4	42:37:20.9	-22.0	21.3	<9.3[b]
	02:24:47.1	42:01:25.4	-20.8	21.5	9.8

Table 7—Continued

Cluster	RA (J2000)	Dec (J2000)	M_R	$P_{1.4GHz}$ log[W Hz^{-1}]	L_{FIR} log[L$_\odot$]
	02:24:53.3	43:19:29.1	-21.8	22.0	<9.3[a]
	02:25:16.3	42:05:21.7	-22.4	21.7	9.7
	02:26:05.1	42:08:37.1	-22.3	22.1	10.1
	02:26:46.3	41:50:02.7	-21.5	22.0	10.5
	02:26:53.2	41:41:24.4	-21.5	21.5	9.9
	02:26:55.0	42:00:58.5	-20.8	21.4	<9.2[a]
	02:27:31.4	41:55:51.8	-21.3	21.8	10.5
	02:27:34.7	41:58:40.0	-21.8	22.2	10.7
	02:27:36.8	42:00:26.6	-21.4	21.5	10.5
	02:29:01.1	42:41:42.9	-20.5	21.3	10.0
	02:29:24.5	40:25:45.7	-20.4	21.3	<9.1[b]
	02:31:12.9	43:21:28.9	-20.8	21.8	9.8
	02:31:14.3	40:23:24.9	-21.6	21.8	10.1
	02:35:24.9	40:52:09.5	-22.5	22.2	10.3
	02:38:05.6	41:47:22.1	-21.8	21.7	10.0
A397	02:53:02.0	15:11:41.0	-20.6	21.8	10.2
	02:54:01.8	14:58:27.9	-22.6	23.0	11.3
	02:55:28.0	15:48:32.5	-20.2	21.7	<9.7[b]
	02:56:14.4	17:08:21.1	-21.0	21.9	10.3
	02:56:27.9	16:00:28.7	-21.7	22.7	10.1
	02:56:34.7	16:53:04.0	-21.6	21.7	<9.8[b]
	02:56:53.8	16:48:43.7	-21.0	<22.6	<10.0[a]
	02:57:04.6	15:58:59.3	-21.7	22.2	10.3
	02:57:25.7	15:28:17.5	-21.4	21.8	<10.0[a]
	02:58:35.6	16:05:16.2	-21.3	21.9	10.2
	02:59:22.2	16:15:31.4	-20.7	21.9	<9.9[a]
	02:59:58.5	16:35:00.9	-20.9	22.1	10.5
A400	02:53:31.3	06:28:24.0	-21.2	21.8	10.1
	02:53:37.7	06:03:38.2	-20.4	21.5	<9.9[a]
	02:53:58.8	05:59:15.4	-21.0	21.5	<10.1[a]
	02:54:03.6	06:15:26.7	-21.2	21.5	<10.0[b]
	02:54:34.6	05:15:05.6	-20.6	21.7	<10.2[a]

Table 7—Continued

Cluster	RA (J2000)	Dec (J2000)	M_R	$P_{1.4GHz}$ log[W Hz^{-1}]	L_{FIR} log[L$_\odot$]
	02:56:17.7	04:31:45.4	-20.7	21.6	$<9.8^a$
	02:56:28.4	04:36:37.4	-21.0	21.6	10.0
	02:56:42.1	05:59:36.4	-20.1	21.8	$<10.0^b$
	02:56:43.2	07:19:59.7	-21.9	21.7	10.2
	02:56:45.9	06:03:17.2	-20.2	21.6	$<10.1^a$
	02:56:56.7	06:12:19.3	-21.2	21.9	10.3
	02:57:41.7	06:01:27.7	-22.4	24.8	9.9
	02:58:28.6	06:12:20.3	-20.5	21.8	$<9.8^a$
	02:58:29.8	06:18:21.9	-21.5	22.1	10.4
	02:59:16.2	06:07:59.6	-21.0	21.8	9.9
A426	03:07:47.9	41:22:31.4	-21.3	21.6	$<9.8^a$
	03:10:08.5	42:49:48.4	-21.7	23.9	9.6
	03:10:13.0	40:45:56.3	-22.1	21.9	10.3
	03:13:10.3	42:59:50.8	-20.7	21.4	10.0
	03:13:57.7	41:15:24.2	-21.6	22.4	9.7
	03:14:09.9	40:37:18.5	-20.4^c	21.7	10.4
	03:14:31.9	42:46:15.6	-21.8	21.7	$<9.5^b$
	03:14:40.5	39:37:03.2	-21.8	21.6	10.2
	03:15:01.4	42:02:08.5	-22.1	22.8	10.8
	03:16:00.7	40:53:10.0	-21.9	21.4	10.1
	03:16:43.0	41:19:29.3	-22.7	23.5	9.8
	03:16:45.9	40:19:47.5	-21.1	21.5	10.1
	03:16:46.7	40:00:12.6	-22.4	22.3	$<9.5^b$
	03:17:51.1	41:27:02.8	-21.6	22.3	$<9.6^a$
	03:17:52.4	43:18:13.7	-21.7	22.1	10.3
	03:18:15.7	41:51:27.7	-22.9	24.5	$<9.4^b$
	03:18:43.3	42:17:59.8	-21.9	21.9	10.3
	03:18:45.3	43:14:19.7	-21.7	21.5	9.8
	03:18:58.2	41:28:11.4	-22.0	21.9	$<9.3^b$
	03:19:21.4	41:29:25.8	-22.9	21.9	$<9.5^b$
	03:19:34.3	41:34:48.9	-21.9	21.9	$<9.5^b$
	03:19:48.3	41:30:41.3	-23.2	25.1	10.7

Table 7—Continued

Cluster	RA (J2000)	Dec (J2000)	M_R	$P_{1.4GHz}$ log[W Hz^{-1}]	L_{FIR} log[L$_\odot$]
	03:19:51.6	41:34:23.7	-22.1	21.2	<9.4[b]
	03:19:54.2	41:33:47.2	-22.6	21.5	<9.4[b]
	03:20:12.2	41:22:00.3	-22.3	21.5	<9.4[a]
	03:20:22.0	41:38:25.4	-20.8	21.5	<9.5[a]
	03:21:40.0	41:21:36.2	-22.3	21.4	<9.6[a]
	03:22:03.0	40:51:49.4	-22.2	21.3	<9.4[b]
	03:22:05.3	42:10:17.2	-21.1	21.3	<9.3[a]
	03:24:23.0	40:47:19.4	-20.9	22.5	<9.7[a]
	03:24:43.9	41:58:07.9	-21.2	21.8	10.1
	03:25:05.4	40:33:30.3	-21.9[c]	22.3	10.8
	03:25:09.4	42:24:05.3	-21.5	21.4	10.0
	03:25:25.8	40:32:10.0	-21.9[c]	21.9	10.2
	03:25:52.5	40:44:53.7	-21.4	22.1	10.3
	03:25:59.2	40:47:19.8	-22.1	21.5	<9.3[b]
	03:26:00.6	42:01:28.4	-20.1	21.3	9.9
	03:26:34.8	41:41:41.7	-21.1	21.3	9.9
	03:27:47.9	40:02:01.5	-20.5	21.2	9.7
	03:27:55.3	39:59:48.7	-21.1	21.5	9.8
	03:27:59.3	39:54:14.8	-21.4	21.4	9.7
	03:28:27.8	40:09:15.6	-22.0	22.4	10.6
	03:30:01.8	41:49:56.0	-22.0[c]	21.9	10.6
A539	05:13:24.0	07:31:35.0	-20.9	21.6	<10.2[a]
	05:13:30.4	07:25:06.5	-21.2	21.9	<9.9[b]
	05:13:46.3	05:42:54.2	-21.7[c]	22.1	<10.1[a]
	05:14:07.0	06:31:13.5	-22.2	21.9	10.3
	05:14:53.1	06:15:02.2	-21.7	21.7	10.1
	05:15:36.7	07:11:53.7	-21.7	22.0	10.3
	05:15:50.6	06:13:39.1	-21.0	21.9	10.0
	05:16:05.7	05:34:28.4	-21.5	21.8	9.9
	05:16:14.2	06:06:23.7	-21.6	21.9	10.4
	05:16:26.5	06:28:08.4	-22.7[c]	21.8	<10.1[a]
	05:16:26.6	06:50:48.8	-21.1	21.7	<9.6[b]

Table 7—Continued

Cluster	RA (J2000)	Dec (J2000)	M_R	$P_{1.4GHz}$ log[W Hz^{-1}]	L_{FIR} log[L$_\odot$]
	05:16:46.3	06:37:19.7	-21.5	21.8	<10.0[b]
	05:16:55.2	06:33:07.7	-22.6	22.6	<9.8[b]
	05:17:09.9	06:55:36.8	-21.9	21.8	<10.5[a]
	05:19:12.8	05:52:40.4	-21.1	22.0	<10.0[a]
	05:19:33.7	05:25:43.8	-20.8	21.6	<10.0[a]
	05:19:51.5	05:29:59.5	-21.1	21.6	<9.8[b]
	05:20:06.1	06:34:54.7	-21.4	22.0	10.4
	05:20:12.3	05:55:17.9	-21.3	21.7	10.3
	05:20:12.6	05:50:11.5	-21.8	22.5	10.6
	05:21:45.8	06:41:18.5	-22.5	21.9	<10.5[a]
	05:21:49.9	06:40:35.7	-20.9	22.1	<10.5[a]
A569	07:02:33.1	50:35:26.2	-22.0	21.4	9.8
	07:03:03.1	49:25:29.0	-21.7	21.6	9.9
	07:05:42.0	50:34:51.6	-22.8	22.2	9.7
	07:07:51.7	48:24:51.1	-20.1	21.8	<9.3[b]
	07:08:10.9	50:40:55.1	-22.5	21.9	9.8
	07:08:34.2	50:37:52.2	-21.1	21.4	9.8
	07:09:08.0	48:36:56.1	-22.6	23.8	<9.3[b]
	07:09:23.0	48:38:07.9	-22.0	21.6	<9.2[b]
	07:09:34.2	50:10:56.2	-22.4	23.0	<9.2[b]
	07:10:34.2	50:07:07.8	-21.9	21.4	<9.6[a]
	07:11:41.6	49:51:44.1	-22.3	21.8	<9.2[b]
	07:12:43.7	50:03:42.7	-20.8	21.8	<9.1[b]
	07:16:52.3	49:52:29.4	-20.4	21.3	9.8
	07:22:18.6	49:17:32.1	-22.2	21.8	9.8
A634	08:08:44.7	56:35:31.2	-21.3	21.6	9.9
	08:09:39.6	57:31:27.5	-20.5	21.5	<9.6[b]
	08:09:52.6	57:54:44.8	-21.9	21.8	<9.4[b]
	08:11:53.6	57:57:05.3	-21.0	22.2	10.4
	08:11:57.5	58:42:02.9	-21.4	21.7	9.8
	08:12:08.5	57:54:26.7	-20.5	21.7	10.0
	08:12:17.2	58:33:50.6	-21.1	21.9	9.7

Table 7—Continued

Cluster	RA (J2000)	Dec (J2000)	M_R	$P_{1.4GHz}$ log[W Hz^{-1}]	L_{FIR} log[L$_\odot$]
	08:12:50.6	57:55:15.9	-21.6	21.8	9.9
	08:14:15.5	58:11:57.7	-20.1	21.5	9.9
	08:15:44.9	58:19:14.1	-22.6	21.9	10.3
	08:16:01.5	58:20:00.7	-20.7	22.0	10.3
	08:18:10.6	57:45:31.2	-21.2	21.7	9.9
	08:22:02.7	57:18:29.4	-21.3	21.5	<9.6[a]
A779	09:18:35.6	34:33:11.1	-21.3	21.7	9.9
	09:19:17.5	34:00:30.1	-21.0	23.3	<9.1[b]
	09:19:24.2	33:37:26.8	-21.3	21.5	9.6
	09:19:41.4	33:44:18.0	-21.2	21.4	9.9
	09:19:46.6	33:44:57.5	-22.6	21.7	9.9
	09:20:37.0	33:04:29.5	-20.6	21.7	9.9
	09:20:52.7	35:22:05.6	-21.6	21.7	10.0
	09:21:51.5	33:24:06.9	-21.6	23.0	<9.4[b]
A1185	11:04:37.2	28:13:40.6	-22.2	22.1	10.3
	11:05:53.8	28:48:00.4	-21.5	21.7	10.1
	11:07:08.7	28:35:32.6	-21.6	22.2	9.9
	11:08:30.3	29:50:13.2	-21.5	21.9	10.2
	11:09:25.8	29:34:09.3	-21.8	21.9	10.0
	11:09:33.1	28:37:39.9	-21.0	21.9	10.2
	11:10:47.8	28:39:37.1	-21.7	22.9	<9.7[b]
	11:10:55.3	28:28:10.3	-21.1	22.0	10.1
	11:10:55.9	28:32:37.5	-22.1	21.9	<9.7[b]
	11:10:59.9	29:20:11.7	-21.3	22.2	9.9
	11:11:13.0	28:42:42.6	-21.7	22.7	11.0
	11:11:13.2	28:41:47.0	-22.1	22.9	11.1
	11:11:19.2	28:40:51.4	-21.2	21.8	11.0
	11:12:04.0	27:34:01.2	-20.8	21.8	<9.7[a]
	11:13:10.4	27:49:05.7	-22.2	21.9	9.8
	11:13:11.3	28:00:43.5	-20.7	21.7	<9.8[a]
	11:16:10.7	29:26:31.8	-21.0	22.0	10.5
A1267	11:24:10.7	27:00:49.9	-21.7	21.8	—

Table 7—Continued

Cluster	RA (J2000)	Dec (J2000)	M_R	$P_{1.4GHz}$ log[W Hz^{-1}]	L_{FIR} log[L$_\odot$]
	11:24:24.0	27:42:44.3	-20.7	22.7	—
	11:28:25.3	27:27:18.8	-20.8	22.2	—
	11:30:28.0	25:48:57.2	-21.0	22.0	—
	11:30:53.4	26:19:27.4	-21.1	22.1	—
	11:31:09.5	26:13:33.5	-21.4	22.4	—
	11:31:45.8	26:28:30.7	-21.3	22.2	—
A1367	11:36:20.1	20:31:17.5	-21.2	21.8	<9.5[b]
	11:36:54.3	19:59:47.9	-21.3	21.4	10.5
	11:36:54.3	19:58:15.3	-21.3	22.2	10.4
	11:40:41.7	20:20:33.7	-22.5	21.6	<9.7[a]
	11:42:24.6	20:07:07.8	-21.4	22.1	10.4
	11:42:56.5	19:57:55.5	-20.4	22.3	<9.5[a]
	11:43:13.3	20:00:16.0	-20.2	21.7	9.6
	11:43:48.6	19:58:11.0	-21.7	22.7	10.3
	11:43:58.2	20:48:21.8	-20.2	21.5	9.8
	11:43:58.3	20:11:05.6	-20.7	21.5	<9.7[a]
	11:43:59.0	20:04:35.9	-21.4	21.6	10.0
	11:44:02.2	19:56:58.1	-22.8	22.1	<9.5[a]
	11:44:47.1	20:07:28.9	-21.9	21.4	9.5
	11:44:47.7	19:46:22.4	-20.1	21.8	10.2
	11:44:49.4	19:47:41.2	-21.9	22.2	10.1
	11:44:52.4	19:27:14.8	-21.3	22.0	10.2
	11:44:54.9	19:46:34.3	-21.0	21.4	10.1
	11:45:04.0	19:58:24.3	-22.3	22.0	9.9
	11:45:05.1	19:36:21.0	-22.3	24.7	<9.4[b]
	11:45:17.7	20:01:09.9	-20.8	21.6	9.9
	11:45:27.8	20:48:24.7	-21.6	22.0	<9.3[b]
	11:45:49.0	20:37:42.0	-20.9	21.5	9.9
	11:45:59.9	20:26:18.8	-21.4	22.2	10.7
	11:46:12.3	20:23:28.6	-21.3	22.1	<9.7[a]
	11:46:46.8	21:16:16.1	-21.1	21.5	9.8
	11:50:52.4	21:10:14.2	-21.6	21.5	10.0

Table 7—Continued

Cluster	RA (J2000)	Dec (J2000)	M_R	$P_{1.4GHz}$ log[W Hz^{-1}]	L_{FIR} log[L$_\odot$]
	11:50:55.6	21:08:42.0	-20.9	21.7	10.1
	11:51:01.2	20:23:56.2	-22.3	21.5	9.9
	11:52:01.3	20:39:31.4	-20.5	21.4	9.7
A1656	12:52:53.7	28:22:14.5	-21.8	22.5	10.5
	12:54:19.1	27:04:03.0	-22.2	22.9	<9.2[b]
	12:56:06.2	27:40:39.2	-20.1	21.8	9.9
	12:56:43.6	27:10:41.4	-21.7	22.8	<9.5[a]
	12:57:24.4	27:29:50.4	-22.7	22.9	<9.2[b]
	12:57:25.4	27:24:15.2	-20.5	21.5	9.4
	12:57:31.3	26:30:42.2	-20.5	21.9	9.9
	12:57:57.9	28:03:39.4	-20.6	21.7	9.5
	12:58:05.6	28:14:32.6	-21.7	22.4	10.3
	12:58:09.4	28:42:29.5	-21.0	21.8	9.8
	12:58:12.8	26:23:46.9	-21.7	22.7	9.6
	12:58:35.3	27:35:45.1	-21.5	21.5	10.0
	12:58:35.4	27:15:51.1	-20.3	21.7	<9.7[a]
	12:58:37.3	27:10:33.3	-20.0	21.8	9.7
	12:59:02.2	28:06:54.5	-20.6	21.9	9.8
	12:59:05.3	27:38:37.5	-21.0	21.6	9.7
	12:59:23.4	27:54:40.8	-21.7	23.6	<9.4[b]
	12:59:35.7	27:57:32.3	-22.9	23.3	<9.3[b]
	13:00:33.8	27:38:13.8	-20.5	21.7	<9.4[a]
	13:00:35.8	27:34:25.4	-20.5	21.4	9.8
	13:00:38.0	28:03:24.7	-20.7	22.4	10.3
	13:00:40.7	28:31:08.6	-20.3	21.9	<9.3[b]
	13:00:56.1	27:47:25.0	-22.5	22.3	10.2
	13:01:24.8	29:18:48.0	-22.5	22.6	10.9
	13:01:25.2	28:40:36.4	-21.2	21.6	9.8
	13:01:33.7	29:07:48.6	-21.8	21.8	<9.3[b]
	13:01:43.5	29:02:39.2	-21.7	21.4	9.9
	13:01:57.7	28:00:19.6	-21.9	21.8	9.4
	13:02:08.0	27:38:52.5	-21.0	21.4	9.9

Table 7—Continued

Cluster	RA (J2000)	Dec (J2000)	M_R	$P_{1.4GHz}$ log[W Hz^{-1}]	L_{FIR} log[L$_\odot$]
	13:02:12.9	28:12:51.9	-20.5	21.4	9.7
	13:03:29.2	26:33:00.0	-21.0	21.6	9.6
	13:04:18.5	28:28:03.6	-20.6	22.3	<9.4[b]
	13:04:22.8	28:48:37.6	-20.7	21.5	9.5
	13:06:17.3	29:03:46.4	-22.2	22.3	10.1
	13:06:36.5	27:52:21.1	-20.8	21.9	10.2
A2162	16:09:43.1	30:27:09.0	-22.0	21.8	9.7
	16:12:34.1	28:19:07.1	-21.3	21.9	10.6
	16:12:35.6	29:29:04.1	-22.7	23.3	<9.7[b]
	16:12:38.9	29:38:36.0	-21.8	22.7	<9.7[b]
A2197	16:21:22.2	40:48:36.4	-20.7	22.0	9.9
	16:21:41.7	40:35:27.2	-20.7	21.8	10.2
	16:22:00.2	40:26:51.3	-21.1	21.8	10.0
	16:23:23.0	41:39:02.9	-21.6	22.1	10.5
	16:28:28.2	41:13:04.4	-21.8	22.5	10.6
	16:29:00.4	41:17:01.8	-22.0	21.8	10.2
A2199	16:20:55.9	39:51:38.6	-20.2	22.2	10.4
	16:21:05.1	39:55:01.1	-21.5	21.6	10.2
A2197/99	16:22:53.9	40:29:45.8	-20.6	22.3	10.2
A2197/99	16:23:16.6	39:55:10.4	-22.5	22.0	10.1
	16:24:17.8	39:12:39.8	-21.5	21.9	<9.4[b]
	16:24:37.2	39:07:38.5	-21.1	22.1	10.6
	16:25:04.8	39:45:29.2	-20.9	<22.8	10.2
A2197/99	16:25:10.4	40:53:33.2	-22.7	23.5	<9.6[a]
	16:25:23.7	38:48:22.4	-20.8	21.8	10.1
A2197/99	16:25:31.5	40:08:12.9	-20.5	22.1	10.2
A2197/99	16:25:44.5	40:28:31.3	-21.2	21.9	10.2
A2197/99	16:25:49.3	40:20:41.5	-21.3	22.4	10.5
A2197/99	16:25:50.0	40:29:18.3	-22.3	22.7	10.2
A2197/99	16:26:14.3	39:58:00.7	-21.6	22.0	10.4
	16:26:37.1	39:07:37.8	-21.0	21.8	10.3
A2197/99	16:27:11.3	40:54:23.2	-20.6	21.9	9.9

Table 7—Continued

Cluster	RA (J2000)	Dec (J2000)	M_R	$P_{1.4GHz}$ log[W Hz^{-1}]	L_{FIR} log[L$_\odot$]
	16:27:22.2	39:06:34.0	-22.0	22.1	10.2
A2197/99	16:28:38.5	39:33:04.4	-23.0	24.8	9.7
A2197/99	16:28:39.6	40:07:23.8	-21.8	22.1^{d}	<9.5^{b}
A2197/99	16:28:42.3	40:07:25.0	-21.5	22.1^{d}	<9.5^{b}
	16:28:58.1	39:19:08.0	-21.2	22.0	10.3
A2197/99	16:29:20.1	39:25:43.1	-21.7	22.3	<9.4^{b}
A2197/99	16:29:44.9	40:48:40.6	-22.8	22.1	<9.4^{b}
A2197/99	16:29:51.1	39:45:58.2	-21.8	21.9	9.5
A2197/99	16:29:57.9	40:37:45.2	-22.6	22.3	9.7
	16:30:32.8	39:23:02.0	-21.0	22.5	10.1
A2197/99	16:30:33.4	39:49:49.1	-21.5	21.7	9.8
A2197/99	16:31:34.6	40:33:54.9	-21.9	21.9	10.2
	16:33:49.8	39:15:46.5	-21.9	22.3	10.3
A2197/99	16:34:52.5	40:11:39.8	-21.2	21.9	10.2
A2634	23:35:50.0	26:59:43.1	-21.6	22.1	10.5
	23:36:25.7	27:56:07.3	-20.5	22.0	10.1
	23:38:16.7	26:52:03.8	-20.0	21.8	<9.9^{a}
	23:38:29.5	27:01:55.1	-22.9	25.1	<9.8^{a}
	23:38:38.9	27:00:40.4	-22.1	<25.1	<9.8^{b}
	23:40:00.9	27:08:00.3	-22.8	23.9	10.1
	23:40:22.2	27:11:04.0	-21.5	23.0	<9.8^{b}
	23:40:42.6	27:10:39.5	-20.9	22.4	10.7
	23:40:46.9	26:50:07.0	-22.3	22.2	<10.0^{b}
	23:42:16.6	28:10:51.8	-20.9	22.3	<10.0^{b}
	23:42:23.1	27:19:53.2	-21.2	22.1	10.4
	23:42:38.5	27:05:28.4	-21.6	21.8	<10.1^{a}
	23:42:46.8	27:17:50.3	-21.7	22.3	10.6
	23:42:50.1	27:32:58.2	-20.0	22.6	10.3
A2634/2666	23:44:01.2	27:42:53.9	-21.8	21.7	10.0
A2666	23:45:07.0	28:12:19.1	-21.4	21.7	9.8
	23:45:32.4	27:21:37.7	-22.1	21.8	10.2
	23:45:47.5	27:20:19.9	-21.3	21.7	10.2

Table 7—Continued

Cluster	RA (J2000)	Dec (J2000)	M_R	$P_{1.4GHz}$ log[W Hz^{-1}]	L_{FIR} log[L$_\odot$]
	23:47:24.6	28:23:35.7	-21.3	22.0	10.3
	23:47:34.4	28:26:06.1	-20.3	22.1	10.4
	23:47:43.3	27:25:36.9	-21.1	22.0	10.2
	23:49:55.3	28:40:04.2	-20.9	22.0	10.2
	23:50:47.5	27:17:15.7	-21.5	21.7	10.0
	23:52:24.7	28:46:22.1	-22.0	22.4	10.6
	23:55:08.0	27:59:07.8	-20.3	21.8	<9.6[a]
	23:55:50.5	26:50:54.3	-20.9	21.6	10.0
	23:57:26.0	26:50:18.2	-20.1	21.9	10.1

[a] Object IR flux densities derived using *xscanpi*. The source was detected at 60μm or 100μm, but not both. The FIR luminosity is estimated using a flux density in the non-detected band equal to three times the rms noise.

[b] Object not detected at either 60μm or 100μm. Upper limit based on three times the rms noise at 60μm or 100μm, as determined from *xscanpi*.

[c] Photometry corrupted by presence of a star inside the aperture.

[d] Pair of galaxies. The NVSS flux likely represents the combination of the two galaxies, and the corresponding power is consequently an upper limit. The galaxy pair may be seen in Figure 1.

Note. — Column legend — (1) ACO cluster designation; (2) RA of cluster radio galaxy; (3) Dec of cluster radio galaxy; (4) Absolute magnitude of cluster radio galaxy, computed for Gunn-Oke aperture; (5) Logarithm of radio power at 1.4 GHz; (6) Logarithm of FIR luminosity, in units of solar luminosities.

This figure "f1abc.gif" is available in "gif" format from:

http://arXiv.org/ps/astro-ph/0101114v1

This figure "f1defg.gif" is available in "gif" format from:

http://arXiv.org/ps/astro-ph/0101114v1

This figure "f1hijk.gif" is available in "gif" format from:

http://arXiv.org/ps/astro-ph/0101114v1

This figure "f1lmno.gif" is available in "gif" format from:

http://arXiv.org/ps/astro-ph/0101114v1

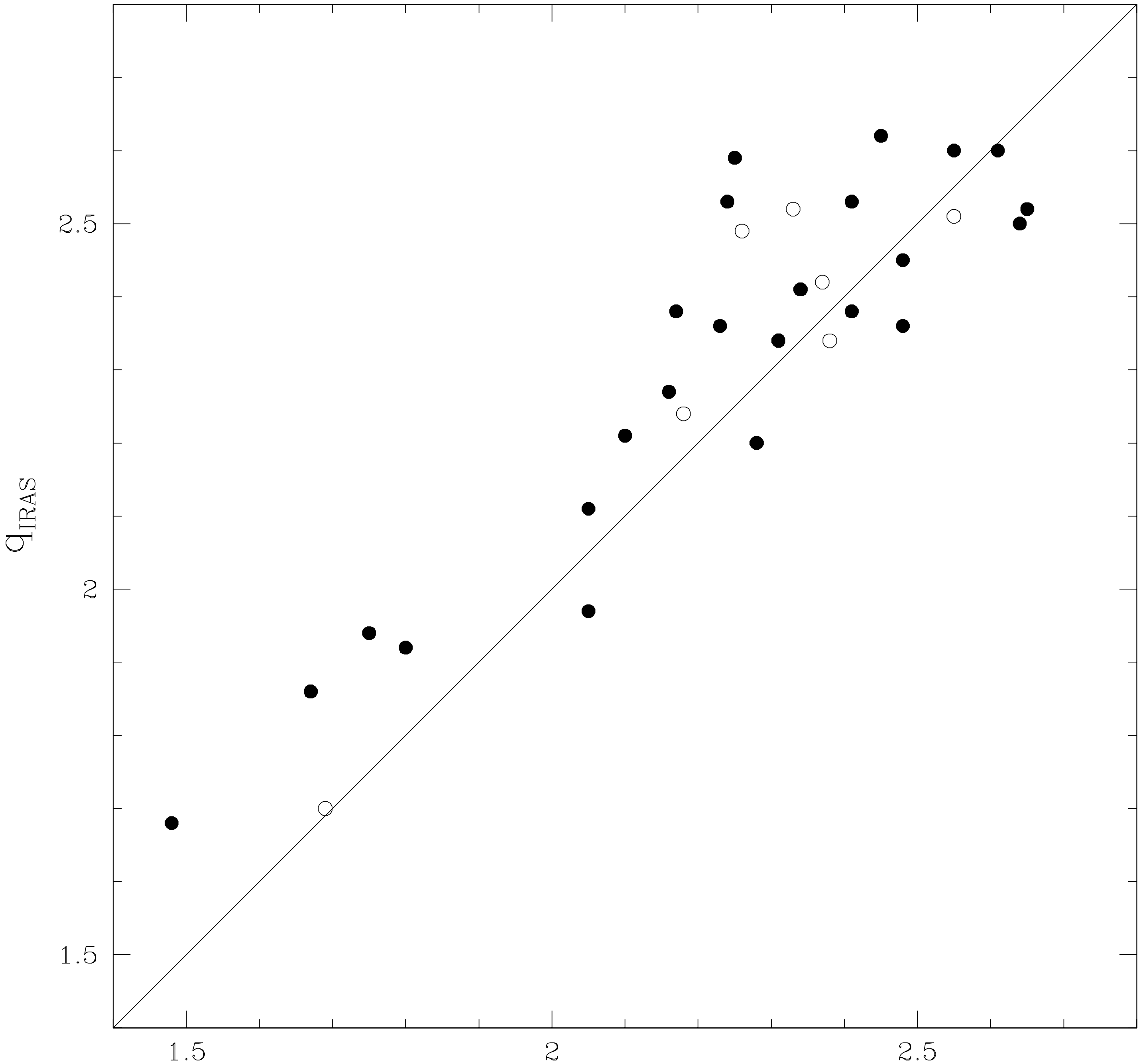
q_IRAS
2.5
2
1.5
1.5
2
2.5
q_scanpi

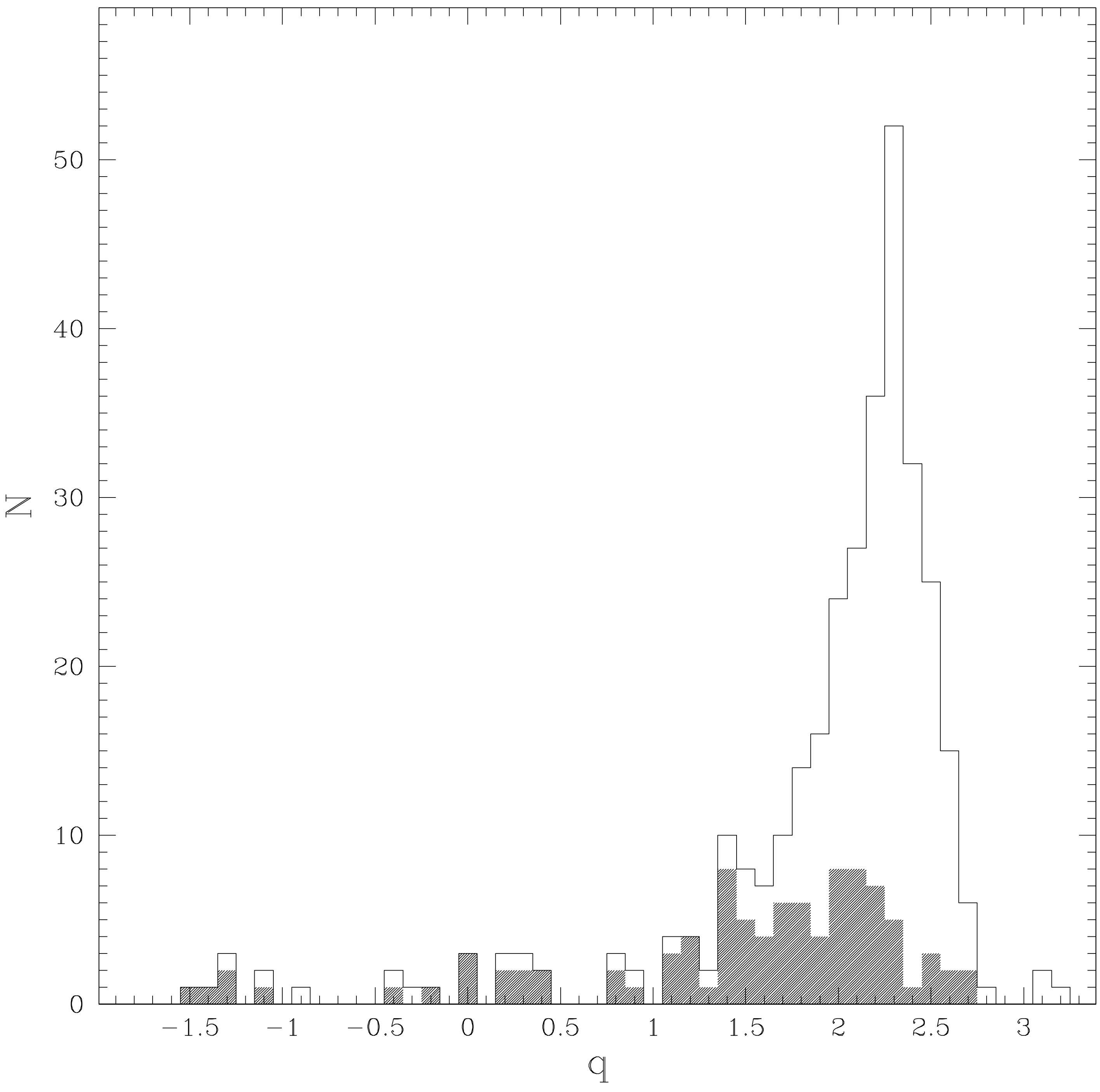
N
0
10
20
30
40
50
−1.5
−1
−0.5
0
0.5
1
1.5
2
2.5
3
q